AD NUMBER

ADB004752

LIMITATION CHANGES

TO:

Approved for public release; distribution is unlimited.

FROM:

Distribution authorized to U.S. Gov't. agencies only; Test and Evaluation; JAN 1975. Other requests shall be referred to Naval Air Systems Command, AIR-954, Washington, DC 20360.

AUTHORITY

usnasc ltr, 4 mar 1977

REPORT NO. 2265.30/470
HAC REF. NO. D0741

Contract N00019–74–C–0127

PATTERN SYNTHESIS OF CONFORMAL ARRAYS

FINAL REPORT

JANUARY 1974 TO JANUARY 1975

Prepared for the AIR SYSTEMS COMMAND
Department of the NAVY

Creating a new world with electronics

HUGHES

ANTENNA DEPARTMENT
AEROSPACE GROUP
HUGHES AIRCRAFT COMPANY
CULVER CITY, CA 90230

Report No. 2265.30/470
HAC Ref. D-0741

PATTERN SYNTHESIS OF CONFORMAL ARRAYS

CONTRACT N00019-74-C-0127

FINAL REPORT

January 1974 to January 1975

Prepared by

P. C. Bargeliotes
A. T Villeneuve
W. H. Kummer
Antenna Department
Radar Microwave Laboratory

Prepared for

Air Systems Command
Department of the Navy
Washington, D. C.

Engineering Division
AEROSPACE GROUPS
Hughes Aircraft Company - Culver City, California

TABLE OF CONTENTS

LIST OF FIGURES

LIST OF FIGURES - Continued

ACKNOWLEDGMENTS

The following personnel of the Hughes Antenna Department contributed to the Pattern Synthesis of Conformal Arrays during this program.

Dr. W. H. Kummer	Program Manager Radar Microwave Laboratory
Dr. P. C. Bargeliotes	Antenna Department
Dr. A. T. Villeneuve	Antenna Department
D. E. Bostrom	Antenna Department
B. J Stevens	Antenna Department

The Authors greatly acknowledge the assistance of Rosalie DeGasperin, Patricia Graham, Genevieve Livingstone and Virginia Schwartz, in the preparation of this report.

The technical officer for this program is Mr. J. W. Willis (AIR-310B).

1.0 INTRODUCTION

The theoretical analysis of exact element patterns from circumferential and radial slots near the tip of a sharply tipped cone has been completed and presented in the final report on Contract No. N0019-73-C-0127 (Bargeliotes, Kummer, and Villeneuve, 1974). In both cases, the element patterns have been obtained by summation of the normal mode series provided by the angular eigenfunctions of the boundary value problem expressed in spherical coordinates. Relatively few modes are required for the convergence of the series for slot locations near the tip of the cone, the number of modes increasing with increased distance from the tip. In addition, computational difficulties from accumulated round-off errors also hinder the applicability of the modal series program for element locations far from the tip.

The normal mode series may be derived from related integrals evaluated as a sum of residues taken over the poles of the integrands (Pridmore-Brown, 1972). This integral representation of the fields lends itself to asympotic approximations which allow the separation of the diffraction field and the geometric optical field. In turn, the diffracted field may be expressed as a product of some frequency-independent angular functions or diffraction coefficients, $\sigma_m(\theta, \theta_o)$, and a function $f(r + a) / (ka)^{1/2}$. Here θ_o is the exterior cone angle, $\underline{a}$ is the distance from the tip to the slot measured along the generatrix, and k is the wave number. The geometry is shown in Figure 1. For slots far from the tip this representation of the diffraction field is better suited for numerical computation than the modal series.

The approximate evaluation of the contour integrals representing the θ-component of the electric field of a circumferential slot resulted in explicit expressions of the field in terms of the diffraction coefficients mentioned above (Pridmore-Brown, 1972). An attempt to utilize these expressions for the numerical computation of the diffraction coefficients and the field itself revealed some inconsistancies or omissions among the given parameters. In an effort to correct these deficiencies, the complete derivation of the expressions was undertaken. Additionally, for a complete pattern analysis or synthesis technique, similar expressions are also required for the diffraction coefficient associated with the ϕ-polarization.

The integral expressions for the scalar potential functions that determine the radiation fields due to a cosmϕ excitation are of the form (Pridmore-Brown, 1972)

$$\int \frac{\nu d\nu}{\nu^2 - \frac{1}{4}} A^m(\theta,\theta_o)\, i^{-\nu} J_\nu(ka)$$

where the angular factor $A_\nu^m(\theta,\theta_o)$ is a ratio of associated Legendre functions and the integrals are taken over a hairpin contour enclosing the positive real axis in the complex ν-plane. On displacing the contour to the right over a large number of poles as shown in Figure 2,we have a finite sum of residues and a contour integral in which the Legendre functions are replaced by their asymptotic representations to order $1/\nu$ with $\nu >> 1$. In the finite sum of residues the Bessel function is replaced by an asymptotic representation, while in the contour integral its Sommerfeld integral representation is used. The Bessel function contour (noted as C_γ in Figure 3 is displaced so as to pass through

the two saddle points at $\gamma = 0$ and $\gamma = \pi$ in the complex γ-plane. As noted by Pridmore-Brown, the contribution from the poles that are crossed in this process and the encountered branch cuts yield the optical and transition fields. The saddle point integrations give terms proportional to $(ka)^{-1/2}$. These terms and the finite residue sum are then transformed into an equivalent modified residue series. The number of terms in the residue series is then allowed to increase without limit. The resulting series is summed in the Cesaro sense and represents the field diffracted by the tip.

It should be noted that in the above method of evaluation of these integrals (Pridmore-Brown, 1972) the condition ka >>N>> 1 is imposed. Here ka is the location of the slot relative to the tip of the cone and N is the number of poles over which the hairpin contour is shifted to the right. Subsequently, N is allowed to increase without limit, which requires that ka also increase without limit if the initial condition ka >>N>> 1 is to be satisfied. In fact it must increase proportional to N^2. Thus, performing the limiting operation would appear to make all terms but the optical term negligible. Therefore it is recognized that interpretation of the results obtained here is not clear. Even so, Pridmore-Brown obtained numerical results for the θ-component of the field that were in very good agreement with results computed from the modal series even for moderate values of ka. The exact reason for this good agreement is not yet understood, but should be investigated further. In addition, the possibility of using a similar approach, but without letting N approach infinity should be investigated in an effort to extend the applicability of the results to even smaller values of ka.

In this report, the analysis of Pridmore-Brown is reviewed, some typographical errors are corrected and some additional details are supplied. We shall begin by first giving the formal defining equations of both components of the electric field in Section 2. We shall also point out here the necessary corrections and omissions in the supporting equations leading to the final expression of the θ-component of the electric field.

In Section 3, the analysis is extended to apply to the ϕ-component of the electric field, resulting in the separation of this field component into transition and diffraction fields. It is found that, unlike the θ-component, the ϕ-component is not represented by an optical term, whereas the diffraction coefficients have the same variation in ka for both components. Throughout the above two sections we follow very closely the formulation and analysis presented by Pridmore-Brown (1972) and the companion paper (Pridmore-Brown, 1973). The same notation will be used throughout unless specifically stated otherwise. Some algebraic details and transformations associated with the various integrations will be included in the appendices.

Also during this program, the radiation patterns of circumferential and radial slot elements 6.22 wavelengths from the tip of a cone were measured at a frequency of 10.38 GHz. A number of the measured patterns are shown together with corresponding computed patterns in Section 4. The computed patterns were obtained from the modal series computer program. Except for a few discrepancies which are explained, the agreement between measured and computed patterns is very good for both the circumferentially and the radially directed element.

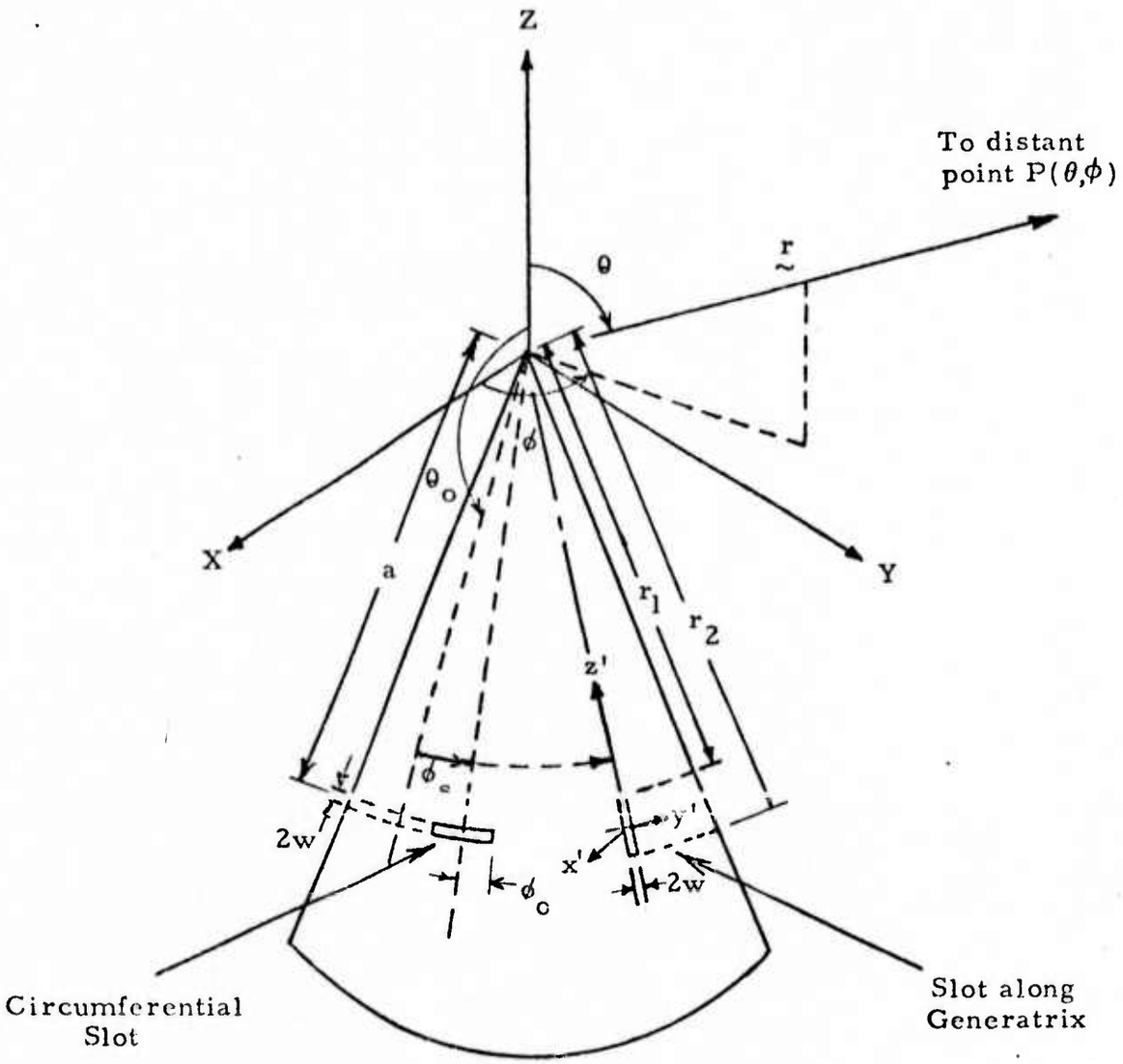

Figure 1. Conical Geometry and Slot Coordinates

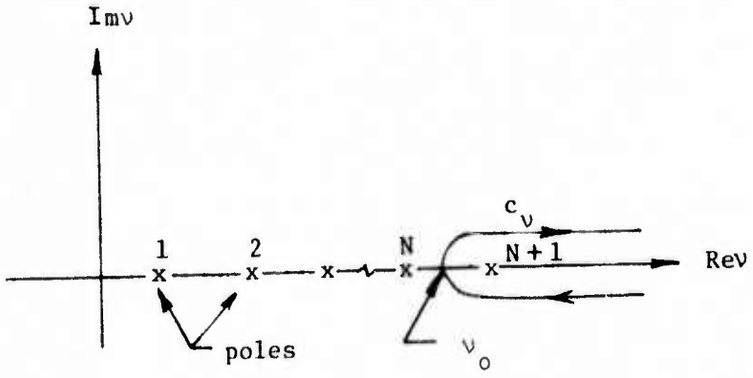

Figure 2. Displaced Hairpin Contour c_ν.

2.0 GENERAL FORMULATION OF THE ASYMPTOTIC APPROACH

The geometry under consideration is a perfectly conducting conical surface coinciding with the coordinate surface $\theta = \theta_o$ of a spherical coordinate system r,θ,ϕ as shown in Fig. 1. A narrow azimuthal slot located at $r = a$ is excited by an alternating voltage

$$V_o \cos m\phi \exp(-i\omega t) \tag{1}$$

The external field generated by this excitation is given by

$$\bar{E} = \text{curl curl } (r\Pi_1) + k \text{ curl } (r\Pi_2) \tag{2}$$

where Π_1, and Π_2 are scalar potential functions and are given by equations (3) and (4) of Pridmore-Brown (1972). The field components are obtained from equation (2), giving

$$E_\theta = \frac{V_o}{r} (2\pi ka)^{\frac{1}{2}} \cos m\phi \exp[i(kr - \pi/4)] P_\theta \tag{3}$$

where

$$P_\theta = P_{1\theta} - \frac{im^2}{\sin\theta \sin\theta_o} P_{2\theta} \tag{3a}$$

$$P_{1\theta} = -\frac{1}{2\pi i} \int_{C_\nu} \frac{\nu d\nu}{\nu^2 - \frac{1}{4}} A_{i\nu}'(\theta,\theta_o)\, i^{-\nu} J_\nu(ka) \tag{3b}$$

$$P_{2\theta} = -\frac{1}{2\pi i} \int_{C_\nu} \frac{\nu d\nu}{\nu^2 - \frac{1}{4}} A_{2\nu}(\theta,\theta_o)\, i^{-\nu} \mathcal{J}_\nu'(ka) \tag{3c}$$

$$A_{1\nu}(\theta,\theta_o) = \frac{P^{-m}_{\nu-\frac{1}{2}}(\cos\theta)}{P^{-m}_{\nu-\frac{1}{2}}(\cos\theta_o)} \tag{4}$$

$$A_{2\nu}(\theta,\theta_o) = \frac{P^{-m}_{\nu-\frac{1}{2}}(\cos\theta)}{(\partial/\partial\theta)\ P^{-m}_{\nu-\frac{1}{2}}(\cos\theta)\Big|_{\theta_o}} \tag{5}$$

$$\mathfrak{J}_\nu(x) = \left(\frac{x}{ka}\right)^{\frac{1}{2}} J_\nu(x) \tag{6}$$

and

$$E_\phi = \frac{V_o}{r}\ \sqrt{2\pi ka}\ \ m\ \sin m\phi\ \exp[i(kr - \pi/4)]\ P_\phi \tag{7}$$

where

$$P_\phi = \frac{-1}{\sin\theta}\ P_{1\phi} + \frac{i}{\sin\theta_o}\ P_{2\phi} \tag{7a}$$

$$P_{1\phi} = -\frac{1}{2\pi i}\int_{C_\nu} \frac{\nu d\nu}{\nu^2 - \frac{1}{4}}\ A_{1\nu}(\theta,\theta_o)\ i^{-\nu}\ J_\nu(ka) \tag{7b}$$

$$P_{2\phi} = -\frac{1}{2\pi i}\int_{C_\nu} \frac{\nu d\nu}{\nu^2 - \frac{1}{4}}\ A_{2\nu}'(\theta,\theta_o)\ i^{-\nu}\ \mathfrak{J}_\nu'(ka) \tag{7c}$$

The integrals are taken over a hairpin contour enclosing the positive real axis of $\nu > \frac{1}{2}$. (Primes denote derivatives with respect to the argument or with respect to the first argument in the case of two arguments. For clarification, we have also added the subscript θ,ϕ to denote quantities corresponding to E_θ and E_ϕ, respectively.)

The above expressions may also be obtained by inspection from the corresponding azimuthal terms in the modal series expressions, noting the $\exp(j\omega t)$ time dependence which has been assumed in our previous reports. This variation is in contrast to the $\exp(-i\omega t)$ used by Pridmore-Brown.

This difference is accounted for by taking the complex conjugate of the modal series in our previous reports. In addition, the slot dimension in the previous reports introduces a constant multiplier to the fields. Both of these points must be kept in mind in any comparison between our previous modal series results and the results from the present analysis.

2.1 On the Transition Field of E_θ

In this section we shall make the necessary corrections to the different expressions given by Pridmore-Brown (1972) and in addition derive some missing quantities necessary for a useful expression of the θ-component. In the following corrections the numbers of the equations used by Pridmore-Brown (1972) are retained for convenience. Equation (13) should read

$$B_{1n}(\theta,\theta_o) = \lim_{\nu\to\nu_n}(\nu-\nu_n)\, A_{1\nu}(\theta,\theta_o) = \left.\frac{P^{-m}_{\nu-\frac{1}{2}}(\cos\theta)}{(\partial/\partial\nu)\; P^{-m}_{\nu-\frac{1}{2}}(\cos\theta_o)}\right|_{\nu=\nu_n} \tag{13}$$

Similarly, the residue of A_{2n} at its nth pole is

$$B_{2n}(\theta,\theta_o) = \lim_{\mu\to\mu_n}(\mu-\mu_n)\, A_{2\mu}(\theta,\theta_o) = \left.\frac{P^{-m}_{\mu-\frac{1}{2}}(\cos\theta)}{(\partial^2/\partial\theta_o\partial\mu)\; P^{-m}_{\mu-\frac{1}{2}}(\cos\theta_o)}\right|_{\mu=\mu_n} \tag{13a}$$

The expression for $\Phi_n(\gamma,\theta)$ below equation (23) should be

$$\Phi_n(\gamma,\theta) = \Gamma^{n+1}\chi_{1n} + \Gamma^{n}\chi_{2n} + \Gamma^{-n}\chi_{3n} + \Gamma^{-n-1}\chi_{4n} \tag{23a}$$

Equation (26) should be multiplied by (-1).

The expression for the complementary error function below equation (27) should be

$$\operatorname{erfc}(z) = \frac{2}{\sqrt{\pi}} \int_z^\infty \exp(-t^2)\, dt \tag{27a}$$

with asymptotic form

$$\operatorname{erfc}(z) = \frac{\exp(-z^2)}{(\pi)^{1/2} z} + 0(z^{-3}) \tag{27b}$$

Equation (35) should be multiplied by (-1). In equation) (30) the arguments of the f and g functions should be $|u|$.

In the evaluation of the first-order contour integral, the deformed C_γ contour must also go around the branch cuts. The branch cut contribution is of comparable magnitude to the rest of the transition field and must be retained in the final expression of the field. A closed form expression for the branch cut contribution is given by the author in the second paper (Pridmore-Brown, 1973). The first-order transition field which is evaluated for small α now becomes

$$I_{1TF}^{(1)} = \int d\gamma \exp(ika \cos) \ln \frac{\alpha}{\alpha-\gamma} + I_{BR}^{(1)}(\alpha)\, H(\alpha)$$

$$= \left(\frac{2\pi}{ka}\right)^{1/2} \exp\left(i\,(ka - \frac{\pi}{4})\right) U(u) + I_{BR}^{(1)}(\alpha)\, H(\alpha) \tag{37a}$$

where $H(\alpha)$ is a unit step function,

$$U(u) = \frac{1}{\sqrt{\pi}} \int_{-\infty}^{\infty} dx \exp(-x^2) \ln(w-x) - \ln w$$

and $I_{BR}^{(1)}(\alpha)$ represents the contribution from the branch cut. The details of the above evaluation are included in Appendix A along with further description of the U(u) function in terms of the plasma dispersion function.

The leading terms in the expansion of the function $A_{1\nu}^{(1)'}(\theta,\theta_o)$ of equation (20) in traveling waves are

$$A_{1\nu}^{(1)'}(\theta,\theta_o) = \left(\frac{\sin\theta_o}{\sin\theta}\right)^{\frac{1}{2}} \left\{\eta_- e^{i(\psi_o + \psi)} - \eta_+ e^{i(\psi_o - \psi)}\right\} \quad (38a)$$

where

$$\eta_\pm \quad \frac{3+4m^2}{8} \cot\theta \pm \frac{1-4m^2}{8} \cot\theta_o$$

The above result of the expansion is used to obtain the complete first-order transition field which includes the contributions from the branch cuts corresponding to α_{10} and α_{20}. The first-order transition field is then

$$P_{1TF}^{(1)} = \frac{i}{4\pi^2}\left(\frac{\sin\theta_o}{\sin\theta}\right)^{\frac{1}{2}} \left\{\Gamma\eta_- I_{BR}^{(1)}(\alpha_{10})\, H(\alpha_{10}) - \eta_+ I_{BR}^{(1)}(\alpha_{20}) - \Gamma\eta_- \sqrt{\frac{2\pi}{ka}}\; e^{i(ka-\frac{\pi}{4})}\; U(u_{10})\right\} \quad (38)$$

where $u_{10} = \left(\frac{ka}{\pi}\right)^{\frac{1}{2}} \alpha_{10}$.

2.2 On the Diffracted Field of E_θ

In the approach used by Pridmore-Brown the diffracted field is given by the Cesàro sum (Wittaker and Watson, 1944) of the residue series. In calculating the Cesàro sum, the terms in the residue series are modified by adding and subtracting terms whose Cesàro sum can be calculated in closed form. This procedure results in a closed form sum plus a convergent

series that can be summed numerically. The terms to be added and subtracted are determined by the following method. The function $B'_{1n}(\theta,\theta_o)$ is first expanded into zeroth-order and first-order terms in $\frac{1}{\nu_n}$. The details of this expansion are shown in Appendix B. The Cesàro sum of these zeroth-order terms is then

$$Q(\theta,\theta_o) = \sum Q_n(\theta,\theta_o) = \sum \frac{1}{\theta_o}\left(\frac{\sin\theta_o}{\sin\theta}\right)^{\frac{1}{2}} \cos \nu_n^{(0)}(\theta_o-\theta)e^{-i\nu_n^{(0)}\pi}$$

$$\xrightarrow[(C,1)]{} \frac{-i}{4\theta_o}\left(\frac{\sin\theta_o}{\sin\theta}\right)^{\frac{1}{2}} \left[\frac{e^{i\mu\alpha}}{\sin\alpha} + \frac{e^{i\mu\beta}}{\sin\beta}\right] \qquad (47)$$

where

$$\alpha = \frac{\pi}{2\theta_o}(\pi - \theta_o + \theta)$$

$$\beta = \frac{\pi}{2\theta_o}(\pi + \theta_o - \theta)$$

$$\mu = -(m + \tfrac{1}{2})$$

Similarly, a closed form for the sum of the first-order terms may be found,

$$R(\theta,\theta_o) = \sum R_n(\theta,\theta_o). \qquad (47a)$$

The individual terms, $R_n(\theta,\theta_o)$, in the above series are obtained from the original first-order expansion by replacing the magnitude factor $1/\nu_n^{(0)}$ by $\theta_o/n\pi$, giving

$$R_n(\theta,\theta_o) = \frac{1}{n\pi}\left(\frac{\sin\theta_o}{\sin\theta}\right)^{\frac{1}{2}} \left[\eta_1 \sin \nu_n^{(0)}(\theta_o-\theta) - i\eta_2 \cos \nu_n^{(0)}(\theta_o-\theta)\right] \cdot \exp(-i\,\nu_n^{(0)}\pi). \qquad (47b)$$

Substituting (47b) in (47a) and carrying out the indicated summation, we find

$$R(\theta,\theta_o) = -\frac{i}{2\pi}\left(\frac{\sin\theta_o}{\sin\theta}\right)^{\frac{1}{2}} \left\{n_1\left(g_1(\alpha,\xi)-g_1(\beta,\xi)\right)+n_2\left(g_1(\alpha,\xi)+g_1(\beta,\xi)\right)\right\} \quad (47c)$$

where

$$g_1(\alpha,\xi) = -e^{-i\alpha\xi}\left[\ln(2|\sin\alpha|) - i\left(\alpha_{\mathrm{mod}\pi} - \frac{\pi}{2}\right)\right]$$

$$g_1(\beta,\xi) = -e^{-i\beta\xi}\left[\ln(2|\sin\beta|) - i\left(\beta_{\mathrm{mod}\pi} - \frac{\pi}{2}\right)\right]$$

ξ = $m - \frac{1}{2}$

α,β defined below Equation (47) above.

A complete expression of E_θ radiation field in terms of the optical, transition, and diffraction fields may now be written from the above results and the results of Pridmore-Brown (1972,1973). Thus,

$$\mathcal{E}_\theta = \cos m\phi \left\{\left(\frac{-\cos\theta_o}{\sin\theta}\right)^{\frac{1}{2}} \left[\exp(ikR) + \Gamma \exp(ikR')\, H(\pi - \theta_o - \theta) + TF\right] + \frac{\exp[ik(r+a)]}{(ka)^{\frac{1}{2}}}\, \sigma_m(\theta,\theta_o)\right\}$$

where

$$\mathcal{E}_\theta = E_\theta \frac{r}{V_o}\left[\frac{2\pi i \cot(\pi - \theta_o)}{ka}\right]^{\frac{1}{2}}$$

$$R = r - a\cos(\theta - \theta_o)$$

$$R' = r - a\cos(\theta + \theta_o)$$

$H(\alpha)$ is a step function, ($H(\alpha) = 1$ for $\alpha > 0$), $\phi \neq 0$.

$$TF = \frac{1}{2\pi} e^{ikr}\left\{i\Gamma\eta_- I^{(1)}_{BR}(\alpha_{10})\cdot H(\alpha_{10}) - i\eta_+ I^{(1)}_{BR}(\alpha_{20}) - \pi e^{ika}\Gamma T(u_{10}) - \Gamma\eta\left(\frac{2\pi i}{ka}\right)^{\frac{1}{2}} e^{ika} U(u_{10})\right\}$$

In the above equation the symbols have the following meanings:

$$\Gamma = i(-1)^m$$

$$\eta_{\pm} = \frac{3+4m^2}{8} \cot\theta \pm \frac{1-4m^2}{8} \cot\theta_o$$

$$I_{BR}^{(1)}(\alpha) = \pi e^{ika\cos\alpha[1+\frac{1}{2}\tan^2\alpha]} \left(\frac{2\pi i}{ka\cos\alpha}\right)^{\frac{1}{2}} \left(\sqrt{\frac{ika\cos\alpha}{2}}\tan\alpha\right)$$

$$T(u) = \left[i^{-u^2}\,\mathrm{erfc}\left(\frac{1-i}{2}\sqrt{\pi}\,|u|\right) - \frac{1+i}{\pi|u|}\right]\mathrm{sgn}(u)$$

$$u = \left(\frac{ka}{\pi}\right)^{\frac{1}{2}} \alpha$$

$$u_{10} = \left(\frac{ka}{\pi}\right)^{\frac{1}{2}} \alpha_{10}$$

$$\alpha_{10} = \pi - \theta_o - \theta$$

$$\alpha_{20} = \pi - \theta_o + \theta$$

$$U(u) = \frac{1}{\sqrt{\pi}} \int_{-\infty}^{\infty} dx\, \exp(-x^2)\, \mathrm{Ln}(w-x) - \mathrm{Ln}w$$

$$w = \left(\frac{ika}{2}\right)^{\frac{1}{2}} \alpha = \left(\frac{i\pi}{2}\right)^{\frac{1}{2}} u$$

$$\sigma_m(\theta,\theta_o) = (2\pi i\cot\theta_o)^{\frac{1}{2}} \left[Q(\theta,\theta_o) + R(\theta,\theta_o) + \sum_{n=1}^{\infty} S_{1n} + \frac{m^2}{\sin\theta\,\sin\theta_o} \sum_{n=1}^{\infty} S_{2n}\right]$$

$$S_{1n} = \frac{\nu_n}{\nu_n^2 - \frac{1}{4}} B_{1n}'(\theta,\theta_o) \exp(-i\nu_n\pi) - Q_n(\theta,\theta_o) - R_n(\theta,\theta_o)$$

Q, Q_n, R, R_n are given by equations (47), (47a), and (47b).

$$B_{1n}'(\theta,\theta_o) = \frac{\left(\frac{\partial}{\partial\theta}\right) P^{-m}_{\nu_n - \frac{1}{2}}(\cos\theta)}{\left(\frac{\partial}{\partial\nu_n}\right) P^{-m}_{\nu_n - \frac{1}{2}}(\cos\theta_o)}$$

$$B_{2n}(\theta,\theta_o) = \frac{P^{-m}_{\mu_n - \frac{1}{2}}(\cos\theta)}{\left(\frac{\partial^2}{\partial\mu_n \partial\theta_o}\right) P^{-m}_{\mu_n - \frac{1}{2}}(\cos\theta_o)}$$

ν_n, μ_n are the roots of $P^{-m}_{\nu - \frac{1}{2}}(\cos\theta_o) = 0$ and $(\partial/\partial\theta_o) P^{-m}_{\nu - \frac{1}{2}}(\cos\theta_o)$, respectively, as in the modal series, and

$$\nu_n^{(0)} = (n\pi - \pi/4 + m\,\pi/2)/\theta_o \qquad n = 1,2,.....$$

The notation Ln denotes the principal value of the logarithm ($|\arg| < \pi$).

It is seen that the diffraction coefficients $\sigma_m(\theta,\theta_o)$ are explicit functions of the coordinates θ,θ_o. It is this property of the diffraction coefficients which makes this analysis attractive for computation of patterns from slots far away from the tip of the cone.

In numerical calculations the seemingly singular point at $\alpha = \pi/2$ of the branch cut function, $I^{1}_{BR}(\alpha)$, is overcome by using the asymptotic form of the defining expression. This gives

$$I^{(1)}_{BR}(\alpha) \approx \frac{2\pi e^{ika\cos\alpha}}{ka\sin\alpha}$$

which at $\pi/2$ becomes $2\pi/ka$ and can be neglected when compared to other items. Also, the function T(u) may be alternatively computed by the expression

$$T(u) = \left[f(|u|) + g(|u|) + i\left[f(|u|) - g(|u|)\right] - \frac{1+i}{\pi\,|u|}\right] \mathrm{sgn}(u)$$

where $f(|u|)$ and $g(|u|)$ are functions related to the Fresnel integrals and have simple rational approximations [Abramowitz and Stegun, 1964.]

As it was pointed out in the introduction, the above expression of the diffracted field has been obtained by allowing N to go to ∞.

$$P_{diff} = \lim_{N \to \infty} (P_{1res} + P_{1sp}).$$

This limiting process disregrrds the condition ka >> N >> 1 imposed at the outset, unless ka is also allowed to go to ∞ faster than N. The field expressions derived by using this limiting process are then used for relatively small values of ka, ka > 10, with satisfactory results over most of the range of θ (Pridmore-Brown, 1972).

At this point an additional comment on the procedure of Pridmore-Brown is in order. In evaluating the zero order integral by the method of steepest descents he separates the result into a so-called saddle point contribution and a transition field that results when a pole exists near the saddle point. The two terms together remain finite when the pole approaches the saddle point. However, separately, each has a singularity at the saddle point. In performing his Cesàro summation, Pridmore-Brown argues that the series containing the contributions from the saddle points gives no contribution to the sum and it is neglected. The remaining transition field now has a singularity when the pole is at the saddle point. However, the Cesàro sum of the residue series provides the proper singularity to cancel the singularity in the transition fields and the resulting fields remain finite. A similar type of thing happens with the first order terms as well. Thus, though his diffraction fields and transition fields each have singularities, the total fields determined by his method remain finite.

It may be possible, however, to separate the diffraction field from the optical and the transition fields without the need to let N to to ∞ by simply adding the non-singular terms of P_{lsp} to the two finite residue sums. The terms of P_{lsp} containing the singularities, (n = 0 terms), are grouped with the transition field. In this manner it may be possible to apply the technique to smaller values of ka than would otherwise be possible. At the same time the singularities in the diffracted field introduced by the limiting process will no longer be present. This alternate approach should be examined further. Also, numerical computations should be undertaken to verify the study results.

3.0 REPRESENTATIONS OF THE E_ϕ-COMPONENT

The formal expressions of the ϕ-component of the electric field are given by equation (7) where the integrals are taken over the hairpin contour enclosing the positive real axis of ν, as was done for the E_θ-component. In comparing the form of the integral expressions of this component with that of E_θ, we see that the only difference is the interchange of the differentiation with respect to θ of $A_{1\nu}$ and $A_{2\nu}$ functions. In view of this similarity, we may proceed with an analysis completely analogous to E_θ as was presented by Pridmore-Brown (1972) and modified in Section 2. For brevity, however, we shall only write down the important end results and definitions, keeping the same basic notation. The notation and meaning of the various quantities shall be the same as for the E_θ-component, except for the identifying subscript ϕ (for ϕ-component) in areas where the distinction is necessary for clarity.

3.1 Representation in Terms of a Shifted Contour

As before, we start by shifting the hairpin contour to the right over N poles, where ka>>N>>1, resulting in a finite sum of N residues and an integral over the contour C_ν shown in Figure 2. In these contour integrals we expand the angularly dependent functions in powers of $\frac{1}{\nu}$, retaining terms up to $0(\nu^{-1})$ in the integrand as was done for the E_θ-component.

Thus

$$P_{1\phi ci} = -\frac{1}{2\pi i} \lim_{\nu_o \to \infty} \int_{C\nu} \nu^{-1} \left[\left(\frac{\sin\theta_o}{\sin\theta} \right)^{\frac{1}{2}} \frac{\sin\psi}{\sin\psi_o} \right] i^{-\nu} \quad J_\nu(ka)\, d\nu \quad (3.1)$$

$$P_{2\phi ci} = -\frac{1}{2\pi i} \lim_{\nu_o \to \infty} \int_{C\nu} \nu^{-1} \left[\left(\frac{\sin\theta_o}{\sin\theta} \right)^{\frac{1}{2}} \frac{\cos\psi}{\cos\psi_o} \right] i^{-\nu} \quad \mathfrak{J}'_\nu(ka)\, d\nu \quad (3.2)$$

where the expansions of $A_{1\nu}(\theta,\theta_o)$ and $A'_{2\nu}(\theta,\theta_o)$ are the expressions in the brackets and

$$\mathfrak{J}'_\nu(ka) = \frac{\nu}{ka} J_\nu(ka) + \frac{J_\nu(ka)}{2ka} - J_{\nu+1}(ka) \quad (3.3)$$

From the above it is evident that the $P_{1\phi ci}$, will result in a first-order contour integral. $P_{2\phi ci}$, on the other hand, will result in a zeroth-order contour integral arising from the first term of (3.3) and a first-order contour integral from the last two terms of (3.3). The first two terms of (3.3), however, vary as $\frac{1}{ka}$ as compared with the other contour integrals and hence may be neglected. This is also the reason why the second contour integral in the E_θ - component goes to zero and does not have any significant contribution to the transition field. We shall consider this next order in ka for the E_ϕ-component only so as to gain some insight into the significance of each of the terms in the final E_ϕ expression.

3.2 Zeroth-Order Contour Integral

By expanding $\frac{1}{\cos\psi_o}$ into traveling waves valid for each of the two sections of the C_ν contour ($Im\nu > 0$, $Im\nu < 0$) and substituting the Sommerfeld integral representation of the Bessel function we find for the zero-order contour integral

$$P_{2\phi ci}^{(0)} = \frac{i}{4\pi^2}\left(\frac{\sin\theta_o}{\sin\theta}\right)^{\frac{1}{2}} \frac{1}{ka} \int_{C_\gamma} e^{ikacos\gamma} \sum_{n=0}^{\infty} \int_{\nu_o} (-1)^n \Phi_n(\gamma,\theta)d\nu \quad (3.4)$$

where $\Phi_n(\gamma,\theta)$ is given by Equation (23a) of Section 2.1. For convenience, we show in Figure 3 the C_γ contour and the deformed contour passing through the saddle points. Figure 3 also shows the location of the simple poles $(\alpha_{10}, \alpha_{20}, \alpha_{30})$ of the zeroth-order contour integral that must be crossed. The indicated branch cuts are associated with the singularities $(\alpha_{10}, \alpha_{20})$ of the first-order contour integrals to be considered in the next section and are taken parallel to the imaginary axis.

We may now write the field arising from crossing the poles and the zeroth-order transition field from the integration along the deformed contour passing through the saddle points as

$$P_{2\phi ci}^{(0)} = \frac{i}{2\pi ka}\left(\frac{\sin\theta_o}{\sin\theta}\right)^{\frac{1}{2}} \left\{ e^{-ikacos(\theta_o-\theta)} + \Gamma e^{-ikacos(\theta_o-\theta)} H(\pi-\theta_o-\theta) - \frac{e^{ika}\Gamma T(u_{10})}{2} \right\} \quad (3.5)$$

where $T(u_{10})$ is defined as before. As in the E_θ case, the contributions from the saddle point at $\gamma = \pi$ for u_{20} and u_{30} cancel one another since $T(u) = -T(-u)$. It is interesting to note that these fields differ by the factor $\frac{i}{ka}$ from the corresponding fields of the E_θ-component.

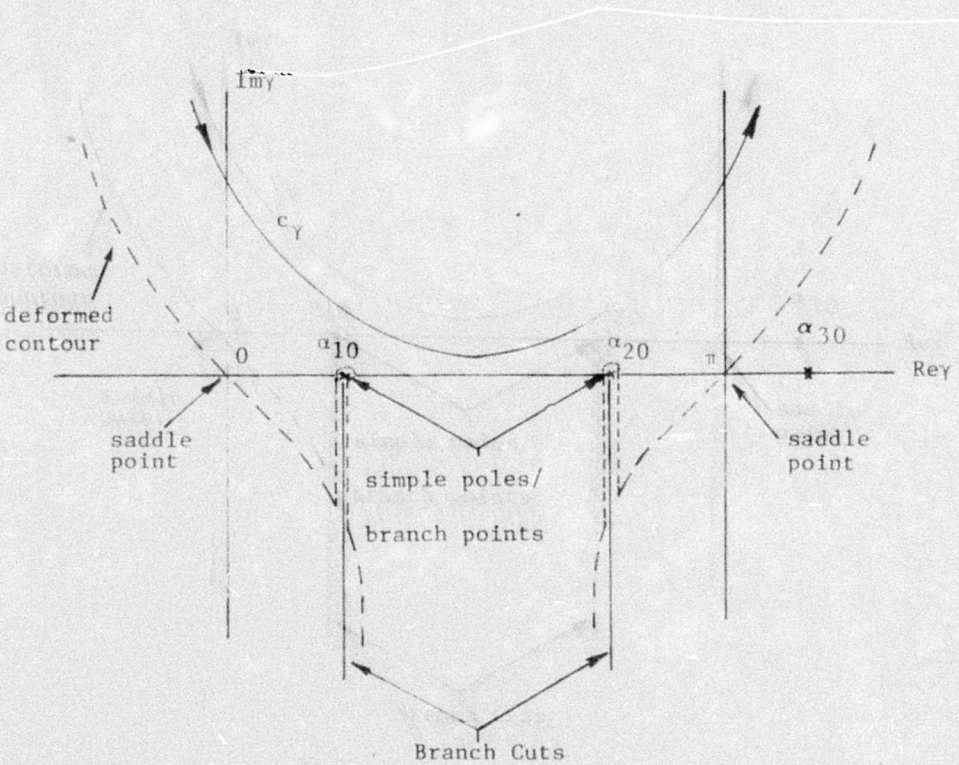

Figure 3. Bessel Function Contour C_γ

We have purposely considered the terms proportional to $(ka)^{-1}$ so that we may compare the different types of fields with the corresponding fields of the θ-component. It is immediately evident that the optical field in this case is not at all significant. Therefore, these terms must be neglected if the θ-component and the φ-component are to be computed to the same order in ka, i.e. $(ka)^{-\frac{1}{2}}$.

3.3 First-Order Contour Integral

In the evaluation of the first-order contour integrals again we make use of the traveling wave expansion of the function $\frac{1}{\sin\psi_o}$ and $\frac{1}{\cos\psi_o}$ for the shifted hairpin contour C_ν. In taking the deformed C_γ contour through the saddle points we encounter branch points associated with the logarithmic singularities of the exponential integrals. The contour integrals associated with J_ν (ka) in $P^{(1)}_{1\phi ci}$ and $P^{(1)}_{2\phi ci}$ give contributions identical to those of the E_θ-component and can be immediately written by analogy. However, the contour integral of $P^{(1)}_{2\phi ci}$ arising from the second factor of (3.3) varies as 1/ka and need not be considered further. Thus,

$$P^{(1)}_{1\phi ci} = \frac{i}{4\pi^2}\left(\frac{\sin\theta_o}{\sin\theta}\right)^{\frac{1}{2}}\left[-\Gamma\ I^{(1)}_{BR}\ (\alpha_{10})\ H(\alpha_{10}) + I^{(1)}_{BR}\ (\alpha_{20}) + \Gamma\sqrt{\frac{2}{ka}}\ e^{i(ka\ -\ \pi/4)}\ U(u_{10})\right] \tag{3.6}$$

$$P^{(1)\ A}_{2\phi ci} = 0 \tag{3.7}$$

The only first-order contour integral of $P_{2\phi ci}$ which is significant (magnitude proportional to $(ka)^{-\frac{1}{2}}$) is the one arising from the last term of (3.3). This contour integral has the form

$$I_{TF}^{(1)B} = \int_{C\gamma} d\gamma\, e^{ikacos\gamma}\, e^{i\gamma} \left[E_1\,(i\nu_o\,(\alpha - \gamma)) - E_1(i\nu_o\alpha) \right], \qquad (3.8)$$

differing from the previous first-order contour integrals by the factor $e^{i\gamma}$ in the integrand. The same process of integration through the saddle points at $\gamma = 0$, $\gamma = \pi$, and around the branch points is carried out as before, giving

$$P_{2\phi ci}^{(1)B} = \frac{-1}{4\pi^2}\left(\frac{\sin\theta_o}{\sin\theta}\right)^{\frac{1}{2}} \left[\Gamma I_{BR\phi}^{(1)}(\alpha_{10}) H(\alpha_{10}) + I_{BR\phi}^{(1)}(\alpha_{20}) - \Gamma\sqrt{\frac{2\pi}{ka}}\, e^{i(ka-\pi/4)} U_\phi(u_{10}) \right.$$

$$\left. - \sqrt{\frac{2\pi}{ka}}\, e^{-i(ka-\pi/4)} \left[U_\phi^*(\bar{u}_{20}) - U_\phi^*(\bar{u}_{30}) \right] \right] \qquad (3.9)$$

It is pointed out that in the above expression we have deleted the phase factor $e^{\pm \frac{i}{2ka}}$. The functions $U_\phi(u)$ and the branch cut contributions $I_{BR\phi}^{(1)}(\alpha)$ differ from their counterparts in the E_θ-component but have essentially the same properties. Unlike the case of the E_θ-component, the above contour integrals through the saddle point at $\gamma = \pi$ for u_{20} and u_{30} result in a net contribution to the field since $U_\phi(u)$ is not an even function of u and hence $U_\phi^*(\bar{u}_{20}) \neq U_\phi^*(\bar{u}_{30})$. If upon further examination this contribution is found to be insignificant, then these factors will not be included in the computation of the field.

3.4 Evaluation of the E_ϕ-Diffracted Field

The diffraction field of the E_ϕ-component is given by the sum of the residue series,

$$\frac{-1}{\sin\theta} P_{1\phi res} + \frac{i}{\sin\theta_o} P_{2\phi res} \longrightarrow P_{\phi diff} \tag{3.10}$$

The residue series $P_{1\phi res}$ and $P_{2\phi res}$ are found from the expansion of the functions $B_{1n}(\theta, \theta_o)$ and $B_{2n}(\theta, \theta_o)$, respectively, and the asymptotic representation of the Bessel functions $J_\nu(ka)$, $J_{\nu+1}(ka)$. Thus,

$$P_{1\phi res} = \sum_{n=1}^{N} \frac{\nu_n}{\nu_n^2 - \frac{1}{4}} B_{1n}(\theta,\theta_o)\, i^{-\nu_n} J_{\nu_n}(ka) \tag{3.11}$$

$$P_{2\phi res} = \sum_{n=1}^{N} \frac{\mu_n}{\mu_n^2 - \frac{1}{4}} B'_{2n}(\theta,\theta_o) i^{-\mu_n} \frac{d}{dx}\left[\left(\frac{x}{ka}\right)^{\frac{1}{2}} J_{\mu_n}(x)\right]_{x=ka} \tag{3.12}$$

where $B_{1n}(\theta,\theta_o)$ and $B_{2n}(\theta,\theta_o)$ are given by (13) and (13a) in Section 2.1. Both residue series converge in the ordinary sense. This summation is accomplished by expanding the coefficients $B_{1n}(\theta, \theta_o)$ in powers of $1/\nu_n^{(0)}$ and $B'_{2n}(\theta,\theta_o)$ in powers of $\frac{1}{\mu_n(0)}$ and retaining the leading term in each expansion. However, on retaining only terms which vary as $(ka)^{-\frac{1}{2}}$, as in the E_θ-component, we are left only with two convergent first-order series denoted by $R_{1\phi}(\theta,\theta_o)$ and $R_{2\phi}(\theta,\theta_o)$ and defined below:

$$R_{1\phi}(\theta,\theta_o) = \sum_{n=1}^{N} R_{1n\phi}(\theta,\theta_o) \tag{3.13}$$

$$R_{2\phi}(\theta,\theta_o) = \sum_{n=1}^{N} R_{2n\phi}(\theta,\theta_o) \tag{3.14}$$

where

$$R_{1n\phi}(\theta,\theta_o) = \left(\frac{\sin\theta_o}{\sin\theta}\right)^{\frac{1}{2}} \frac{\sin\nu_n^{(0)}(\theta-\theta_o)\ e^{-i\nu_n^{(0)}\pi}}{n\pi} \tag{3.15}$$

and

$$R_{2n\phi}(\theta,\theta_o) = \left(\frac{\sin\theta_o}{\sin\theta}\right)^{\frac{1}{2}} \frac{\sin\mu_n^{(0)}(\theta-\theta_o)\ e^{-i\mu_n^{(0)}\pi}}{n\pi} \tag{3.16}$$

are the individual terms in the two series. The details of the expansion of $B_{1n}(\theta,\theta_o)$ and $B'_{2n}(\theta,\theta_o)$ leading to $R_{1n\phi}$, $R_{1\phi}$, $R_{2n\phi}$, $R_{2\phi}$ are included in Appendix B. The diffraction field may be now found by the sum of the two series as

$$P_{diff\phi} = \frac{e^{i(ka-\pi/4)}}{(2\pi ka)^{\frac{1}{2}}}\left\{\frac{-1}{\sin\theta}\left[R_{1\phi}(\theta,\theta_o) + \sum S_{1n\phi}\right] + \frac{i}{\sin\theta}\left[R_{2\phi}(\theta,\theta_o) + \sum S_{2n\phi}\right]\right\} \tag{3.17}$$

where

$$S_{1n\phi} = \frac{\nu_n}{\nu_n^2 - \frac{1}{4}} \frac{P^{-m}_{\nu_n-\frac{1}{2}}(\cos\theta)}{(\partial/\partial\nu)P^{-m}_{\nu-\frac{1}{2}}(\cos\theta_o)\Big|_{\nu_n}} \exp(-i\nu_n\pi) - R_{1n\phi}(\theta,\theta_o) \tag{3.18}$$

$$S_{2n\phi} = \frac{\mu_n}{\mu_n^2 - \frac{1}{4}} \frac{(\partial/\partial\theta)\ P^{-m}_{\mu_n-\frac{1}{2}}(\cos\theta)}{(\partial^2/\partial\mu\partial\theta_o)P^{-m}_{\mu-\frac{1}{2}}(\cos\theta_o)\Big|_{\mu_n}} \exp(-i\mu_n\pi) - R_{2n\phi}(\theta,\theta_o) \tag{3.19}$$

and $R_{1n\phi}(\theta,\theta_o)$, $R_{2n\phi}(\theta,\theta_o)$ are defined by (3.15) and (3.16).

We also have:

$$R_{1\phi}(\theta,\ \theta_o) = \frac{i}{2\pi}\left(\frac{\sin\theta_o}{\sin\theta}\right)^{\frac{1}{2}} \left[g_1(\alpha,\xi) - g_1(\beta,\ \xi)\right] \tag{3.20}$$

$$R_{2\phi}(\theta,\theta_o) = \frac{i}{2\pi}\left(\frac{\sin\theta_o}{\sin\theta}\right)^{\frac{1}{2}} \left[g_1(\alpha,\ \bar{\xi}) - g_1(\beta.\ \bar{\xi})\right] \tag{3.21}$$

$$\nu_n^{(0)} = (n - \tfrac{1}{4} + \frac{m}{2})\ \frac{\pi}{\theta_o}$$

$$\mu_n^{(0)} = (n + \tfrac{1}{4} + \frac{m}{2})\ \frac{\pi}{\theta_o}\ .$$

The functions $g_1(\alpha,\bar{\xi})$, $g_1(\beta,\bar{\xi})$ are obtained from $g_1(\alpha,\xi)$, $g_1(\beta,\xi)$ by replacing ξ with $(\xi+1)$. All other quantities have the same meaning as for the E_θ-component and have been defined in Section 2.3. We are now in a position to express the radiation field of the ϕ-component as a sum of transition and diffraction fields as was done for the E_θ-component. In summing the various fields and normalizing to the same factors as for the E_θ-component, we find

$$\mathcal{E}_\phi = im \sin(m\phi)\left\{\left(-\frac{\cos\theta_o}{\sin\theta}\right)^{\frac{1}{2}} TF_\phi + \frac{\exp[ik(r+a)]}{(ka)^{\frac{1}{2}}}\ \sigma_{m\phi}(\theta,\theta_o)\right\} \tag{3.22}$$

where

$$\mathcal{E}_\phi = E_\phi\ \frac{r}{V_o}\ \left[\frac{2\pi i\ \cot(\pi-\theta_o)}{ka}\right]^{\frac{1}{2}}$$

$$TF_\phi = \frac{\exp(ikr)}{2\pi} e^{-i\pi/2}\left\{\frac{1}{\sin\theta} \cdot \left[-\Gamma\, I^{(1)}_{BR}(\alpha_{10})\cdot H(\alpha_{10}) + I^{(1)}_{BR}(\alpha_{20}) + \Gamma\sqrt{\frac{2\pi}{ka}}\, e^{i(ka-\frac{\pi}{4})}\, U(u_{10})\right]\right.$$

$$+ \frac{1}{\sin\theta_o}\left[\Gamma\, I^{(1)}_{BR_\phi}(\alpha_{10})\cdot H(\alpha_{10}) + I^{(1)}_{BR_\phi}(\alpha_{20}) - \Gamma\sqrt{\frac{2\pi}{ka}}\, e^{i(ka-\frac{\pi}{4})}\, U_\phi(u_{10})\right.$$

$$\left.\left. - \sqrt{\frac{2\pi}{ka}}\, e^{-i(ka-\pi/4)}\left[U^*_\phi(\tilde{u}_{20}) - U^*_\phi(\tilde{u}_{30})\right]\right]\right.$$

$$\sigma_{m\phi}(\theta,\theta_o) = (2\pi i\cot\theta_o)^{\frac{1}{2}}\left[\frac{1}{\sin\theta}\left[R_{1\phi} + \sum S_{1n\phi}\right] - \frac{i}{\sin\theta_o}\left[R_{2\phi} + \sum S_{2n\phi}\right]\right]$$

$$\bar{\alpha}_{20} = \pi - \alpha_{20}$$

$$\bar{u}_{20} = \pi - u_{20}$$

$$\bar{u}_{30} = \pi - u_{30}$$

Also, $R_{1\phi}$, $R_{1n\phi}$, $R_{2\phi}$, $R_{2n\phi}$ are defined by equations (3.13) through (3.16). $U_\phi(u)$ and $I_{BR\phi}(\alpha)$ are given in Appendix A. All other quantities have the same meaning as for the E_θ and may be found in Section 2. As for the E_θ-component, for α near $\pi/2$ the asymptotic form of (A-12) must be used for the numerical computation of $I^{(1)}_{BR\phi}(\alpha)$. This is easily shown to be

$$I^{(1)}_{BR\phi}(\alpha) \qquad \frac{2\pi e^{i(ka\cos\alpha + \alpha)}}{ka\sin\alpha - 1}\ .$$

Since this is of order $0(1/ka)$, the contribution of the branch cut in the vicinity of $\alpha = \pi/2$ can be neglected entirely without affecting the results significantly. It should be noted that the two diffraction coefficients of the θ and ϕ-components have the same variations in ka but in general will have different values at a given point in space.

4.0 MEASURED AND COMPUTED ELEMENT PATTERNS ON A CONE

The computer program which has been developed for conical array pattern analysis has been modified and executed on the Control Data Corporation computer (CDC 6600). The CDC 6600 computer is preferred because of its greater accuracy and higher speed over the IBM 370/158 computer previously used in the pattern analysis problem.

During the course of the development of the modal series program the accurate computation of the Associated Legendre function $P_\nu^m(\cos\theta)$ was questionable over certain ranges of θ. Specifically, the chosen expansion was valid for $\frac{\pi}{6} < \theta < 5\frac{\pi}{6}$ but it was used for computation of the function for $\frac{9}{72+2m} < \theta < \pi$ by first computing $P_\nu^m(\cos\theta)$ with $\nu \simeq 72+2m$. Backward recursion was used to obtain the value of the function of the desired degree. Some details in checking the accuracy of the results in both the upper and lower extension limits of applicability of the expansion are included in the first Quarterly Report (Bargeliotes, 1974).

The computed patterns, using the first fourteen modes of the modal series, have been normalized to the largest value computed for both polarizations for either the circumferential or radial case. Computed and measured elevation cuts are shown on an extended θ -scale to give a single view of the elevation cuts. Since the cone under study has a 10^o half-angle, the position of $\theta=80^o$ was selected for the computed azimuthal cuts. This corresponds to the broadside of the conical surface.

Measurements were made on an experimental 10^{o} half-angle cone at a frequency of 10.38 GHz with the slots 6.22 wavelengths from the cone tip. This slot location corresponds to ka = 39 radians from the cone tip for which a complete set of patterns have been computed with the modal series program. In both the circumferential and the radial case, the slots were fed by a half height X-band waveguide. Where possible, computed pattern values are shown on the same scale for comparison.

4.1 Radiation patterns of circumferential slot.

Figure 4 shows the θ-polarized patterns for $\phi = 0^{o}$ and $\phi = 180^{o}$ together with corresponding computed patterns. There is excellent agreement between the measured and computed patterns throughout the cone tip region and the broadside region where both patterns are quite uniform. The measured pattern drop-off for $\phi = 0^{o}$ and θ greater than 140^{o} is due to shadowing at the base of the cone by the absorbent material in which the cone was set. Similar drop-off is observed in the measured pattern for $\phi = 180^{o}$ for the same θ values except that this is not as noticeable since the computed pattern in this region is at a much lower level relative to the $\phi = 0^{o}$ pattern. Measured θ-polarized patterns are also shown for $\phi = 45^{o}$, $\phi = 225^{o}$ and $\phi = 90^{o}$, $\phi = 270^{o}$ in Figures 5 and 6, respectively. In Figure 6 the corresponding computed pattern values are also shown. There appears to be a 2^{o} difference in the position of the null between the computed and measured patterns but this is probably caused by inaccurate alignment between the transmitter and receiving antennas. This also explains the slight asymmetry in the measured pattern. The shadowing by the absorbent material for θ greater than 140^{o} is evident in all measured patterns. The above two patterns also show that

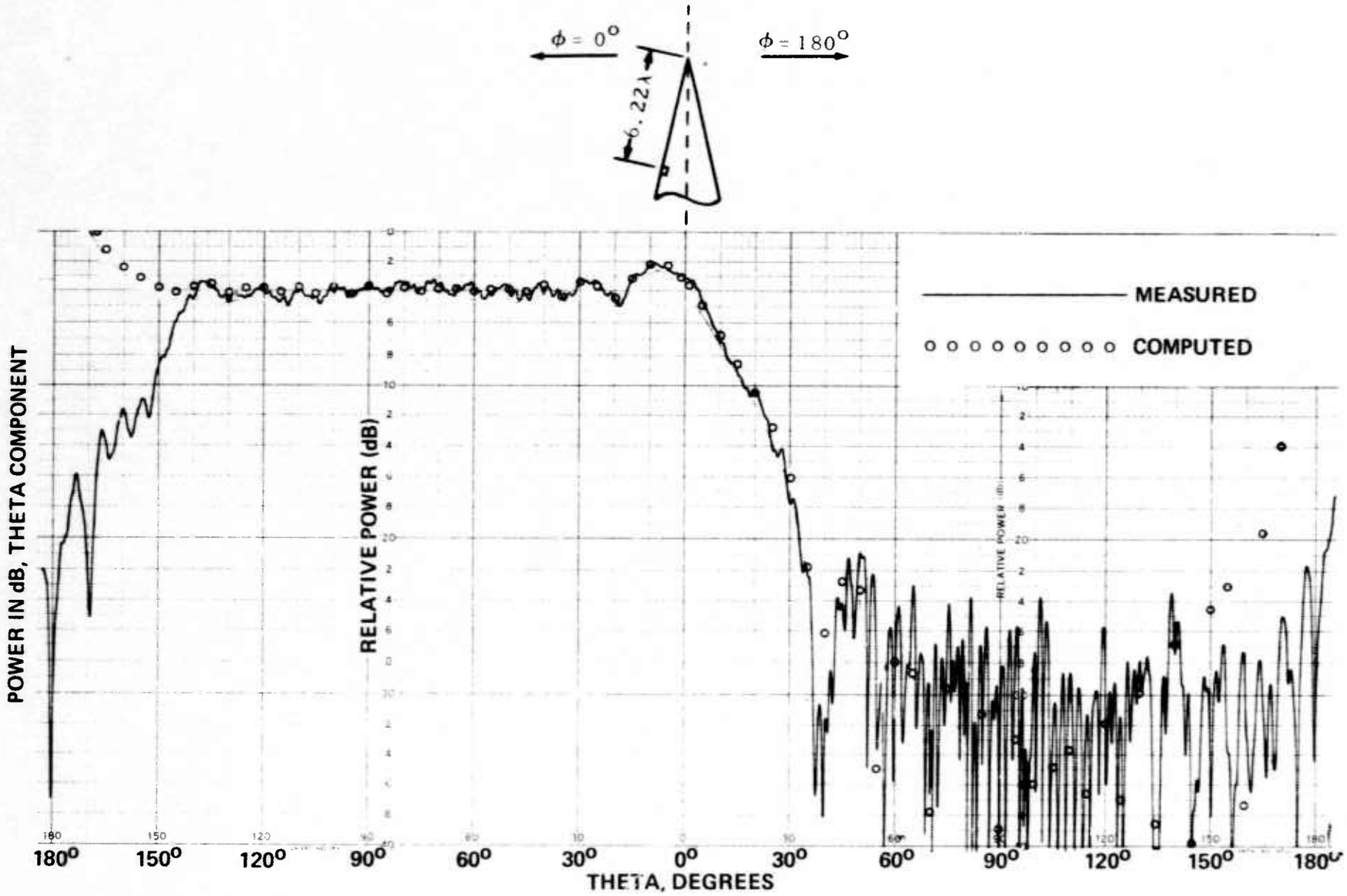

Figure 4. Measured and Computed (M = 13) θ-Polarized Patterns of $\lambda/2$ Circumferential Slot for $\phi = 0^o$, $\phi = 180^o$

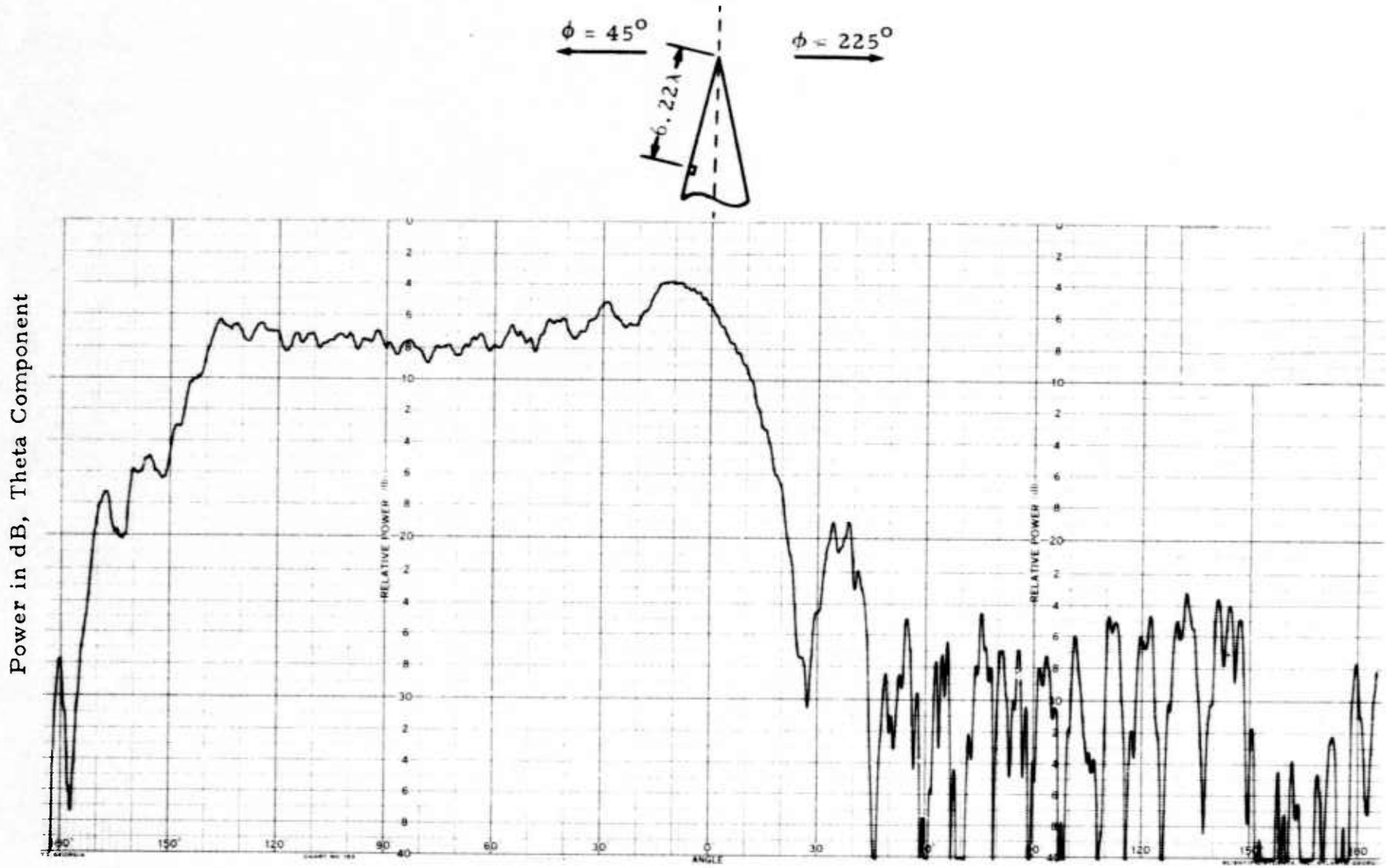

Figure 5. Measured θ-Polarized Patterns of λ/2 Circumferential Slot for $\phi = 45^{\circ}$, $\phi = 225^{\circ}$.

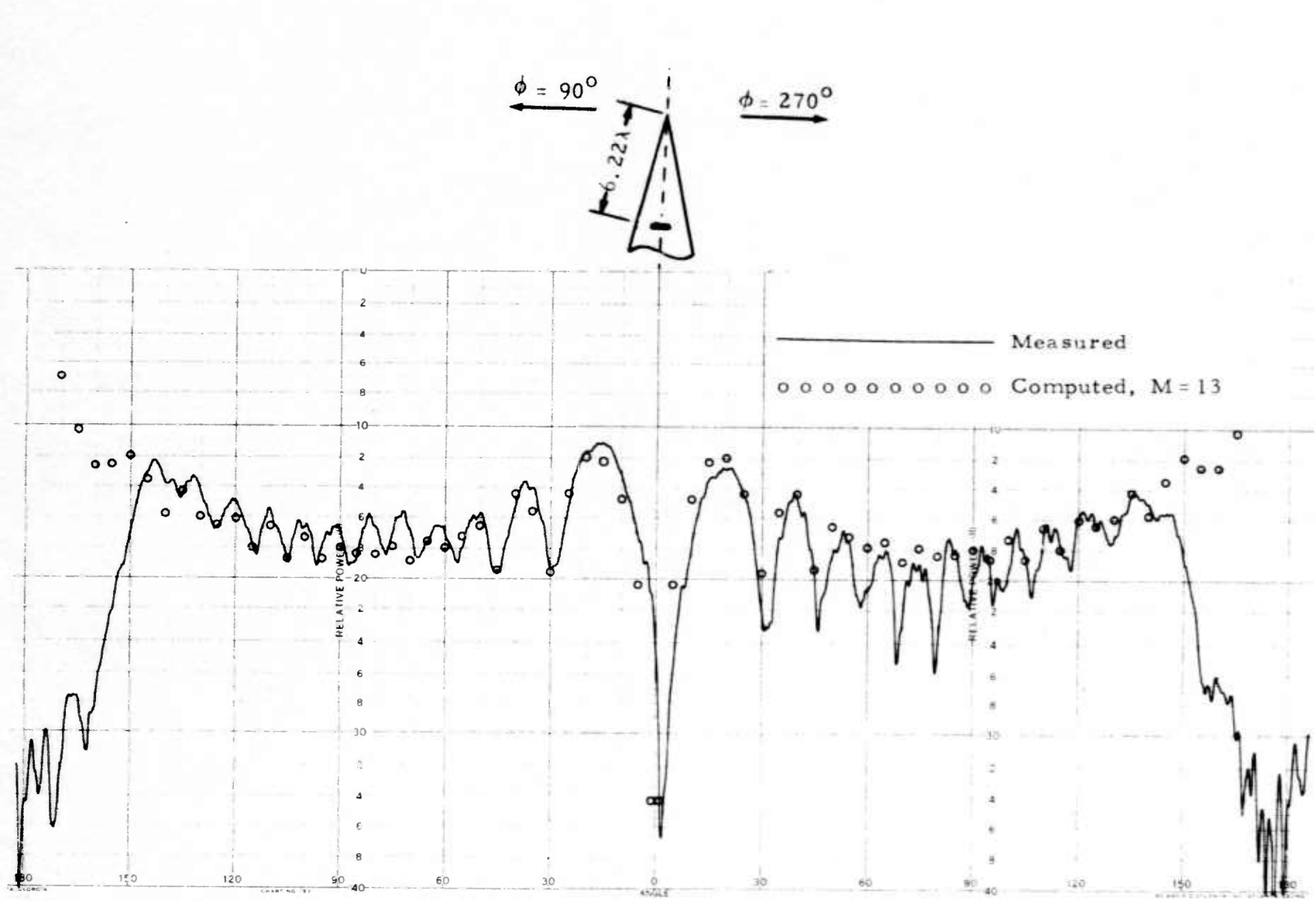

Figure 6. Measured and Computed (M = 13) θ-Polarized Patterns of λ/2 Circumferential Slot for $\phi = 90^\circ$, $\phi = 270^\circ$.

the pattern level at $\phi = 135^{\circ}$ is approximately 10 dB below that of $\phi = 90^{\circ}$.

The ϕ-polarized patterns in elevation are shown in Figures 7 through 9 for the same azimuth positions as for the θ polarized patterns. Azimuthal patterns for both polarizations at $\theta = 80^{\circ}$ are shown in Figure 10. Excellent agreement is seen between computed and measured patterns of Figures 9 and 10 considering the fact that computed pattern values were made every 5 degrees in θ and 10 degrees in ϕ.

4.2 Radiation patterns of radial slot.

The tip section of the 10° half-angle cone was modified to accommodate a radial slot 6.22 wavelengths from the cone tip. The edges of the waveguide were carefully taped to obtain one-half wavelength at the operating frequency. A photograph of the cone mode with a radial slot and absorbent material surrounding the base of the cone is shown in Fgiure 11.

The computed patterns shown together with the measured patterns have been normalized to the largest value computed for both polarizations using the first fourteen modes of the modal series. This largest value was computed at the field point $P(\phi,\theta) = P(0^{\circ},80^{\circ})$. As expected, this point is broadside to the conical surface and lies on the plane normal to the conical surface and containing the radial axis of the slot element. For meaningful comparison of measured and computed patterns, the reference level of the measured patterns was also taken at broadside at $\phi = 0^{\circ}$.

Figure 12 shows the ϕ-polarized patterns for $\phi = 0^{\circ}$ and $\phi = 180^{\circ}$ together with corresponding computed patterns. There is excellent agreement between the measured and computed patterns throughout the cone tip region and the broadside region where both patterns are quite broad.

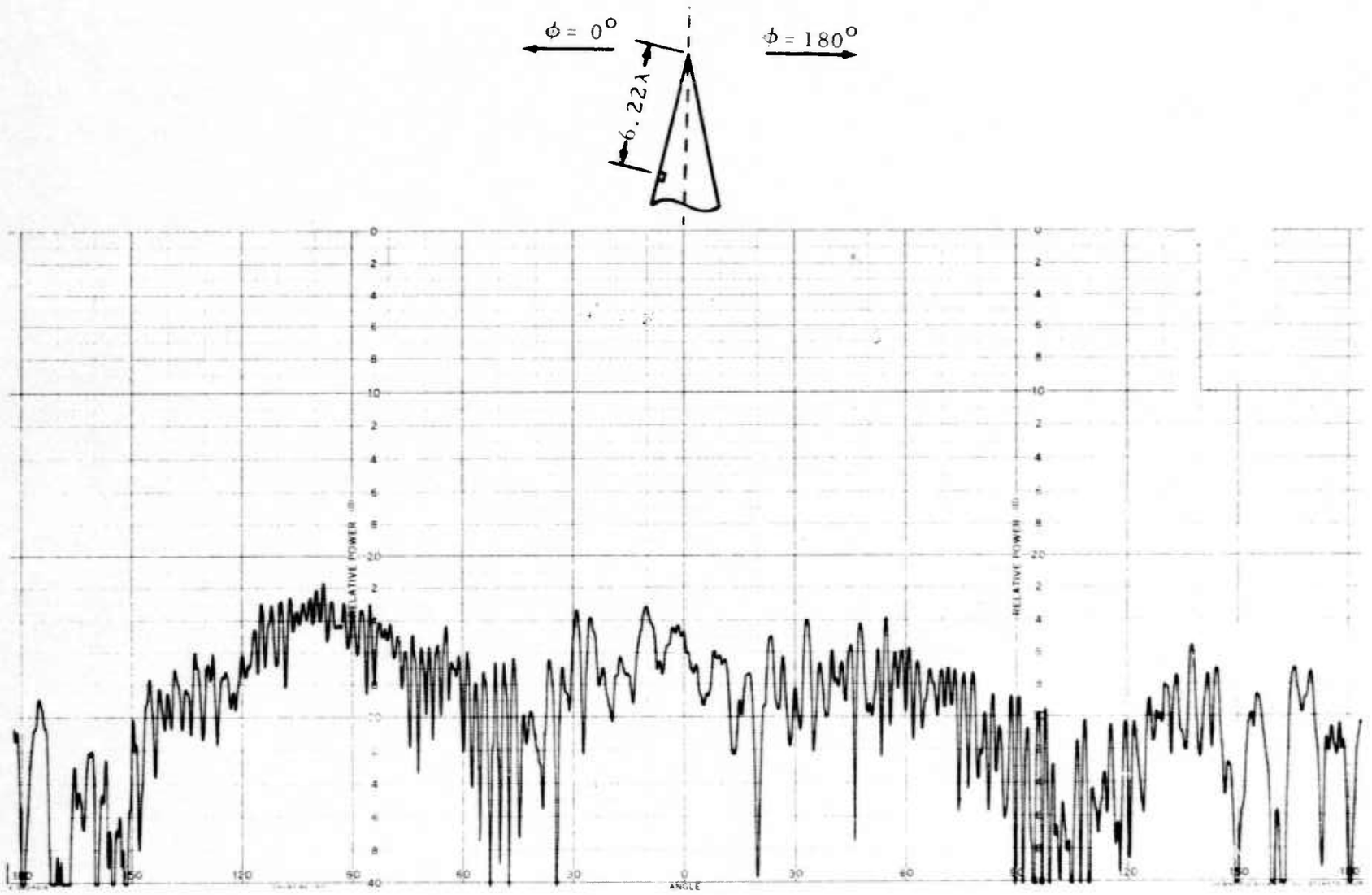

Power in dB, Phi Component

Theta, Degrees

Figure 7. Measured ϕ-Polarized Patterns of $\lambda/2$ Circumferential Slot for $\phi = 0^\circ$, $\phi = 180^\circ$.

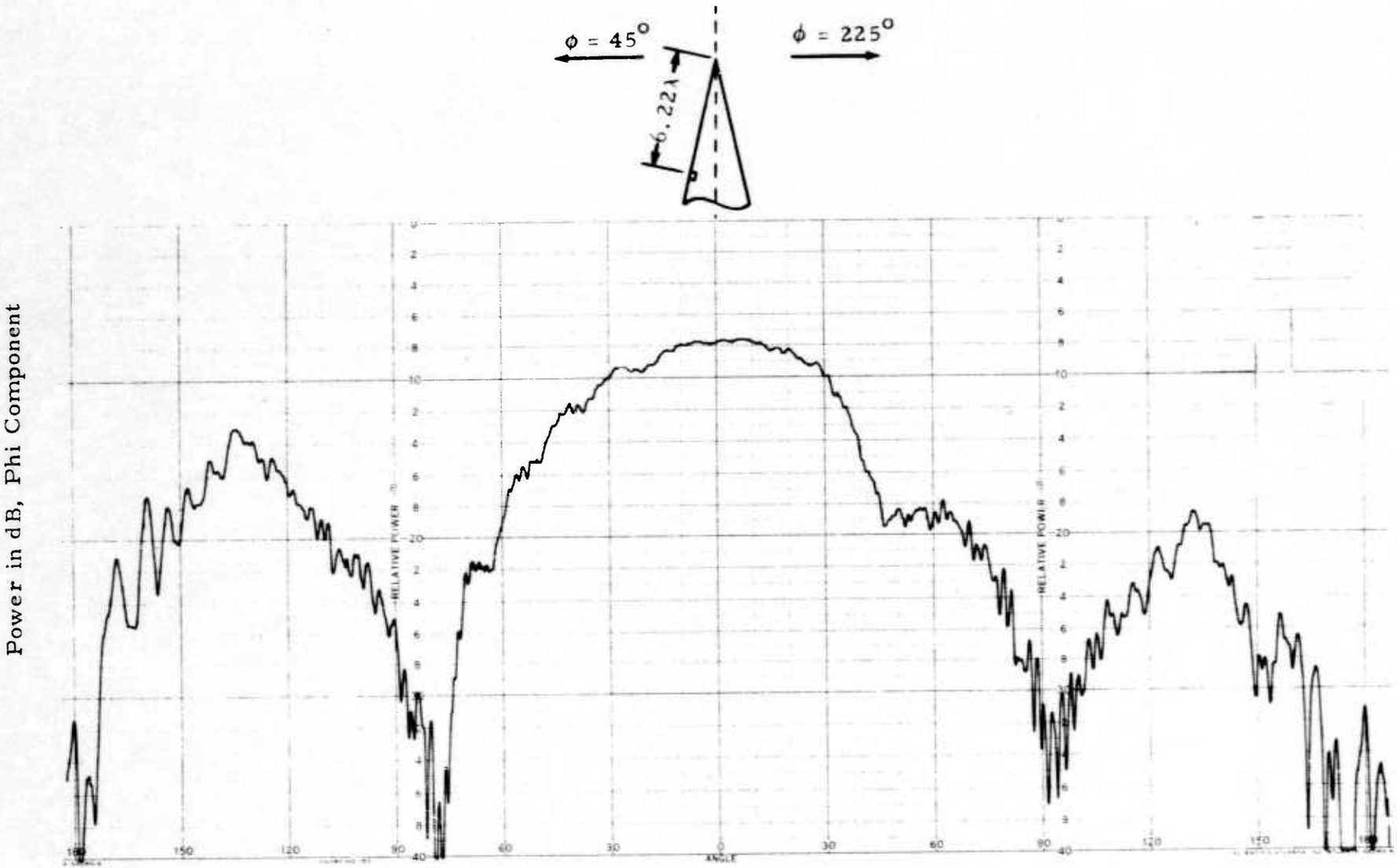

Figure 8. Measured ϕ-Polarized Patterns of $\lambda/2$ Circumferential Slot for $\phi = 45^{\circ}$, $\phi = 225^{\circ}$

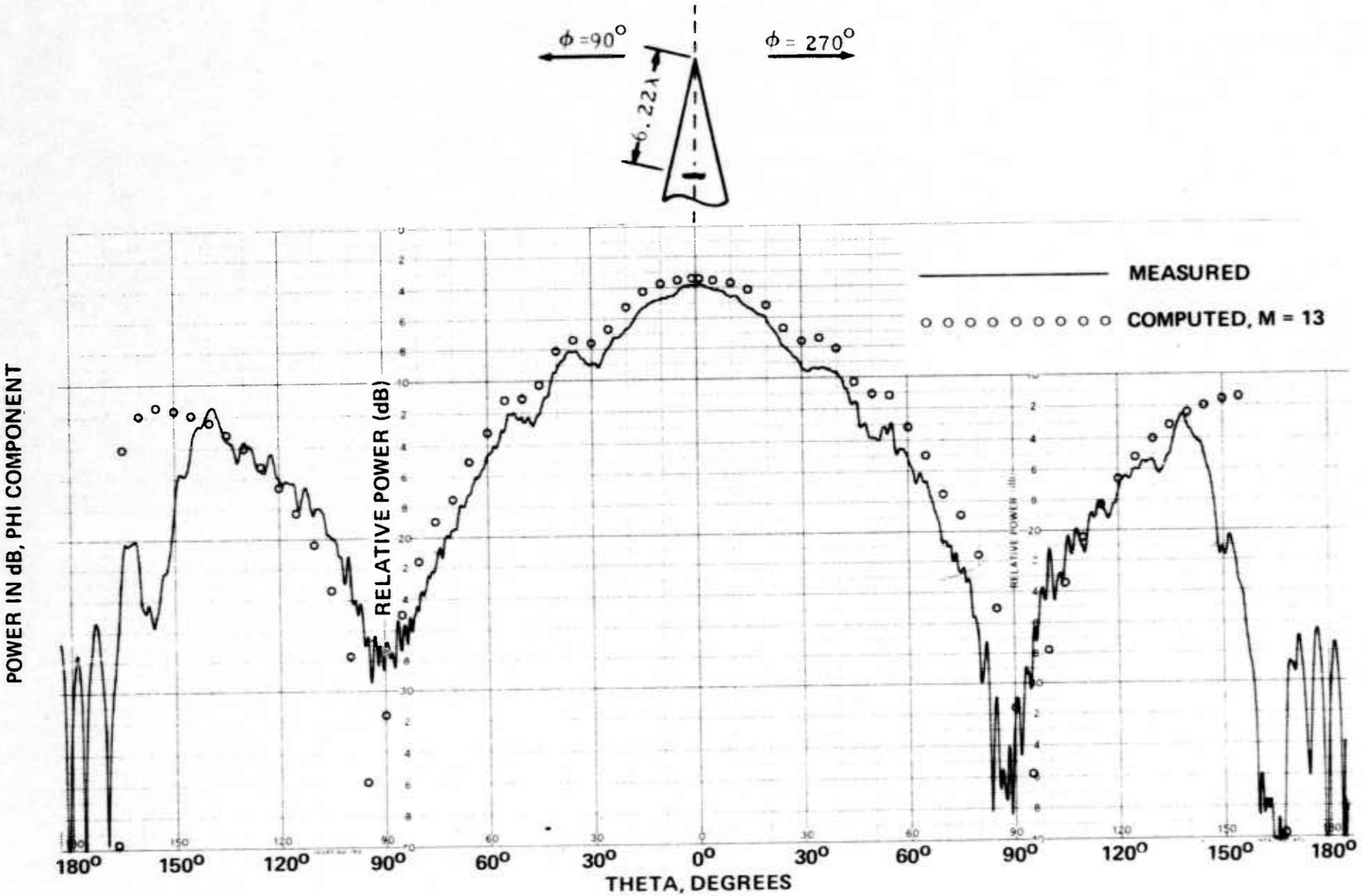

Figure 9. Measured and Computed (M = 13) ϕ-Polarized Patterns of λ/2 Circumferential Slot for $\phi = 90^{\circ}$, $\phi = 270^{\circ}$.

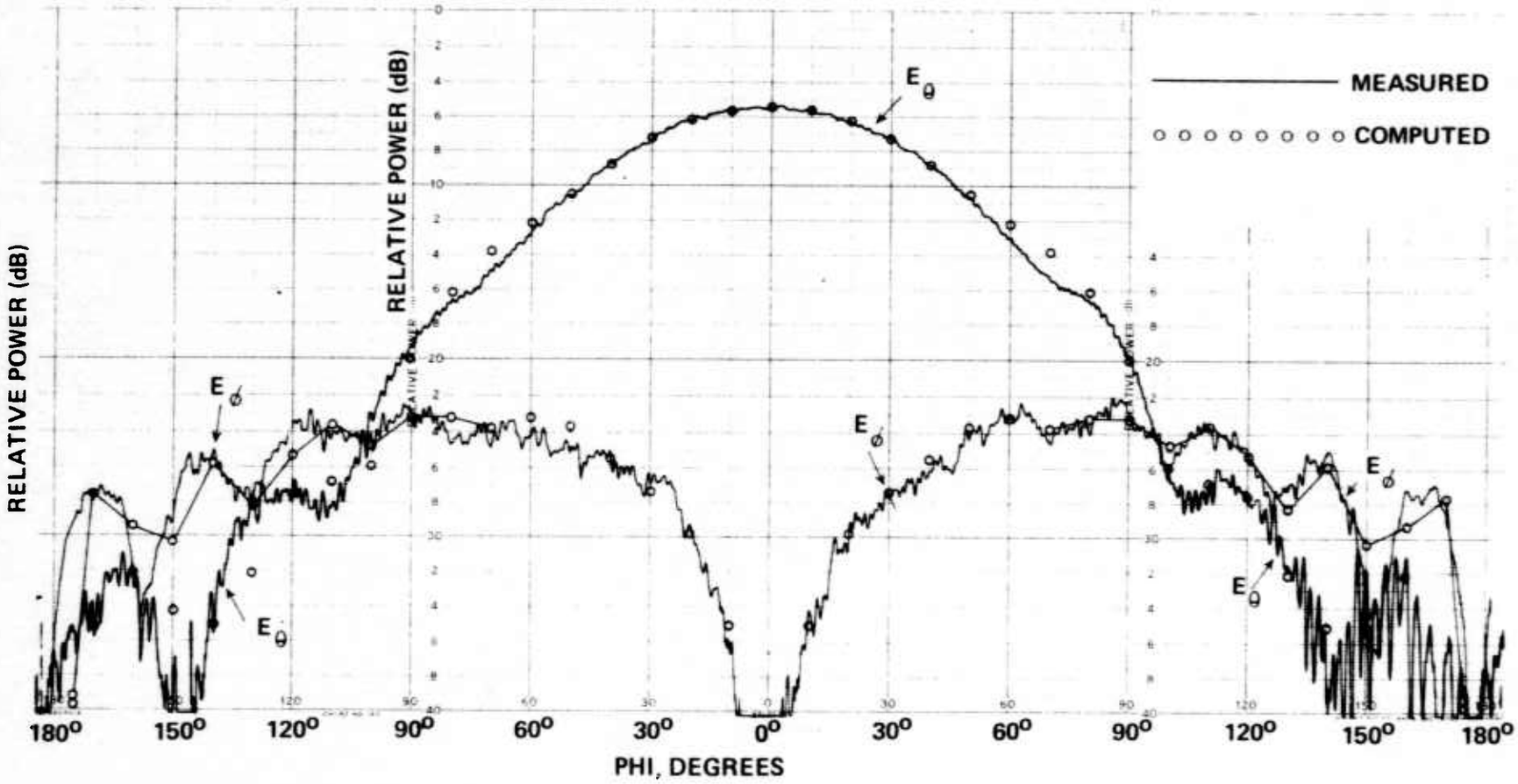

Figure 10. Measured and Computed (M = 13) Patterns of $\lambda/2$ Circumferential Slot for θ and ϕ Polarizations at $\theta = 80^\circ$.

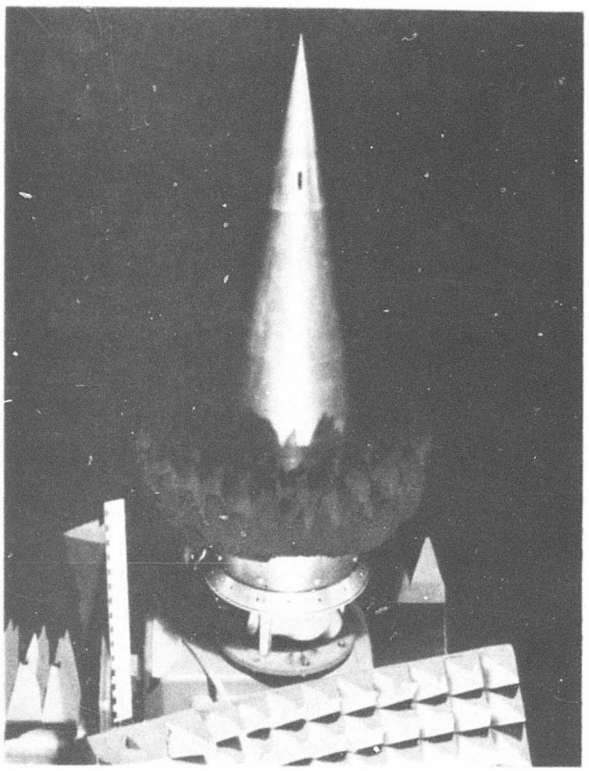

Fig. 11 Test Model of 10^{o} Half-Angle Cone with Slot 6.22λ from Tip

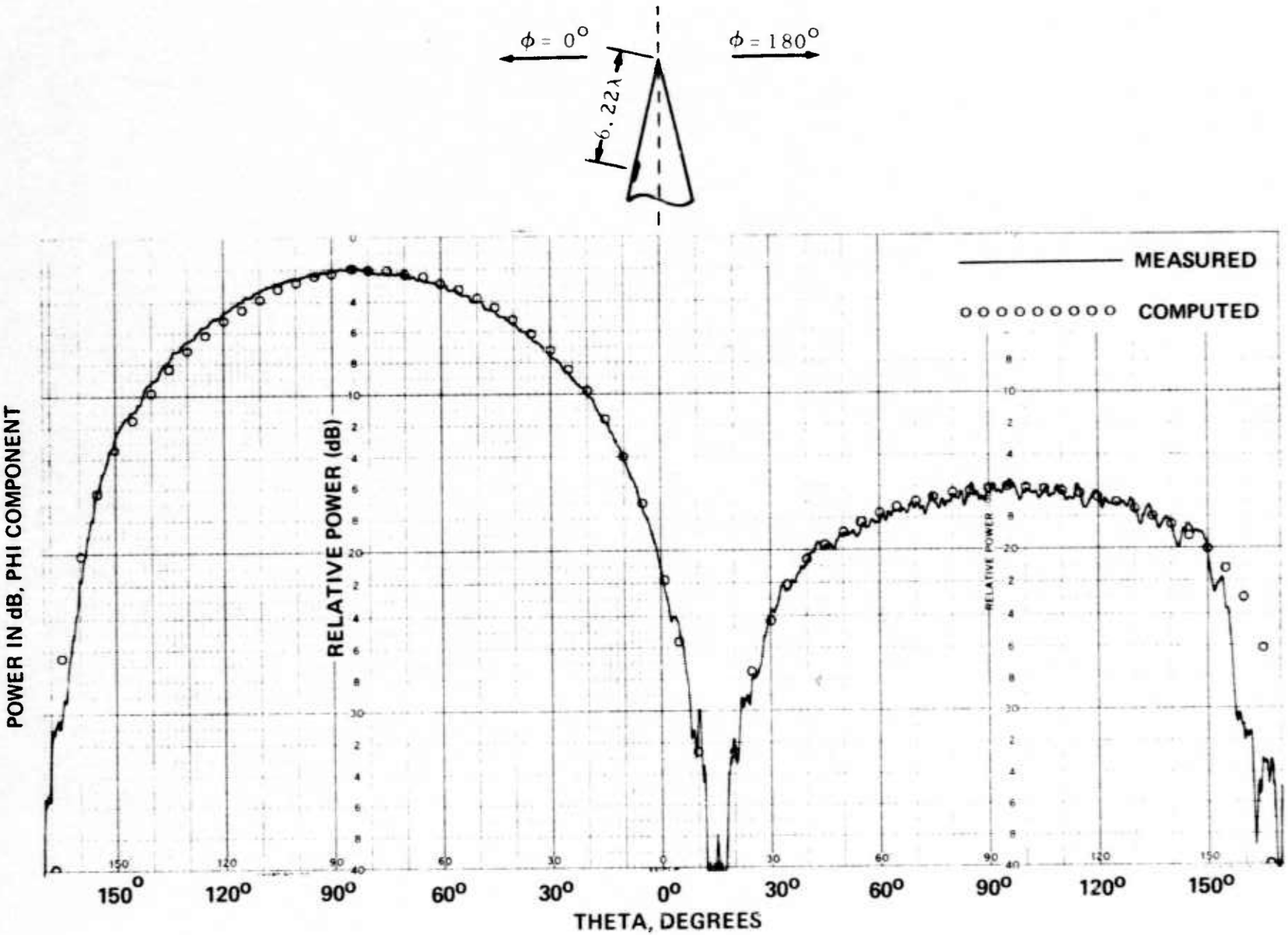

Figure 12. Measured and Computed (M = 13) ϕ-Polarized Patterns of $\lambda/2$ Radial Slot for $\phi = 0^o$, $\phi = 180^o$

Measured ϕ-polarized patterns are also shown for $\phi = 10^{\circ}$, $\phi = 190^{\circ}$, $\phi = 40^{\circ}$, $\phi = 220^{\circ}$, $\phi = 90^{\circ}$ and $\phi = 270^{\circ}$ in Figures 13 through 15. Computed pattern values are also shown in the same figures for comparison. Figure 15 shows a 3° difference in the position of the null between the computed and measured patterns but this is probably caused by misalignment between the transmitter and receiving antennas. It would also explain the slight asymmetry in the measured pattern. The shadowing by the absorbent material for θ greater than 140° is again evident here. The above figures also show that there is a difference of 4 dB in the maxima of $\phi = 0^{\circ}$ and $\phi = 90^{\circ}$ patterns, whereas the pattern maxima at $\phi = 180^{\circ}$ are approximately 14 dB below that at $\phi = 0^{\circ}$. As mentioned earlier, the maxima occur at the broadside to the conical surface.

The θ-polarized patterns in elevation are shown in Figures 16 through 19 for the same azimuth positions as for the ϕ-polarized patterns. These figures clearly show that unlike the patterns of a circumferential slot on a similar cone, the cross-polarization is well below the dominant polarization at the same azimuthal angles. The shadowing by the absorbent material at the base of the cone is clearly identified in these patterns. Since the pattern levels of this polarization are approximately 18 dB below the reference level, the misalignment of the transmitter and receiver antennas is also more apparent.

Azimuthal cuts at various angles, including the broadside of the antenna element, are shown for both polarizations in Figures 20 through 24. From Figure 21 it is seen that the measured broadside pattern of the ϕ-polarization exhibits a broad maximum at $\phi = 0^{\circ}$ and is in very good agreement with the computed pattern. As stated earlier, this has been selected as the reference point for all patterns. In the θ-polarized azimuthal cuts, where the levels are considerably lower than the reference level, the shift of the null between measured and computed patterns is more apparent. At other points, however, the agreement between measured and computed values is very good. The θ-polarized pattern levels are in all cases at least 18 dB below the reference level.

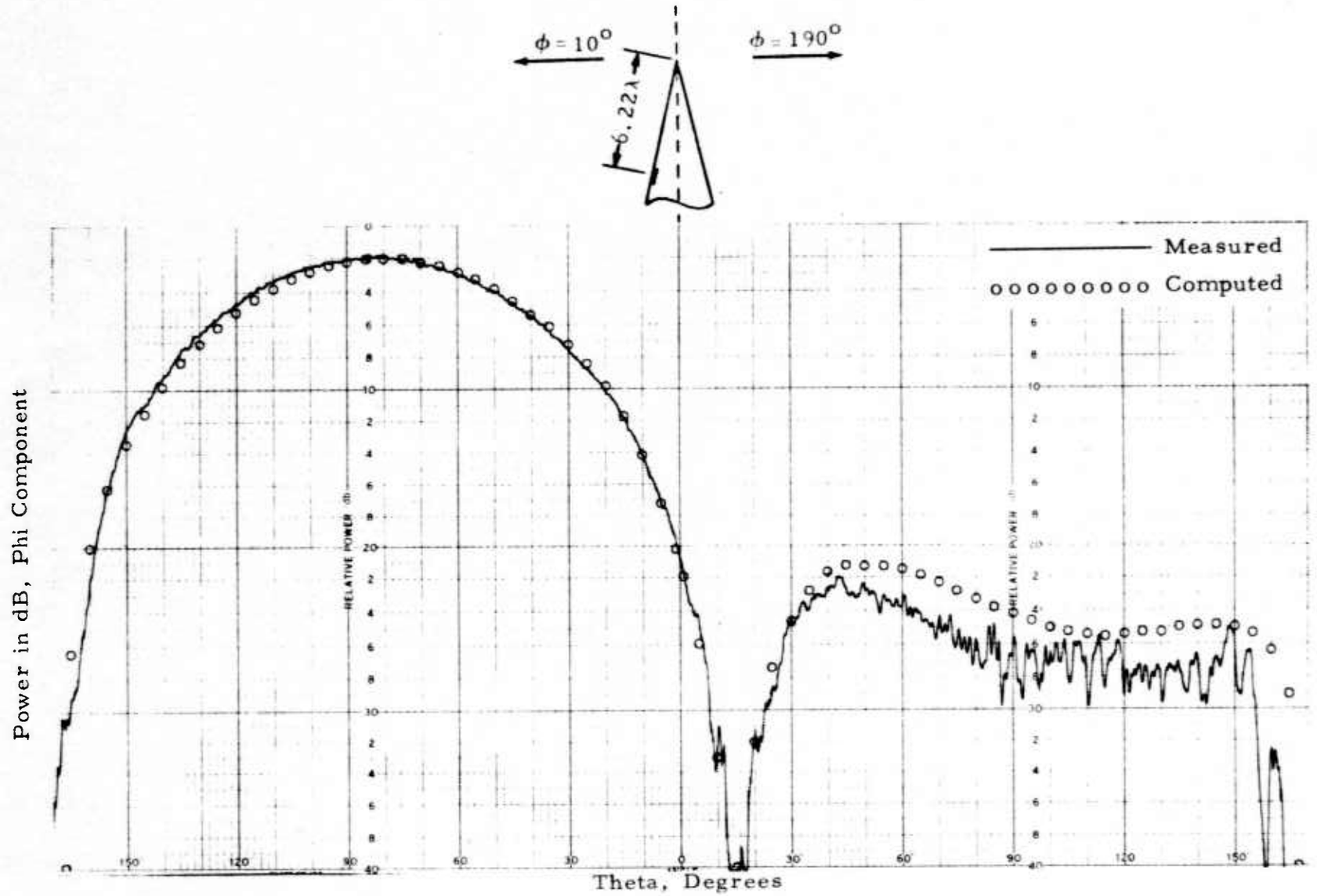

Figure 13. Measured and Computed (M = 13) ϕ-Polarized Patterns of $\lambda/2$ Radial Slot for $\phi = 10^{o}$, $\phi = 190^{o}$

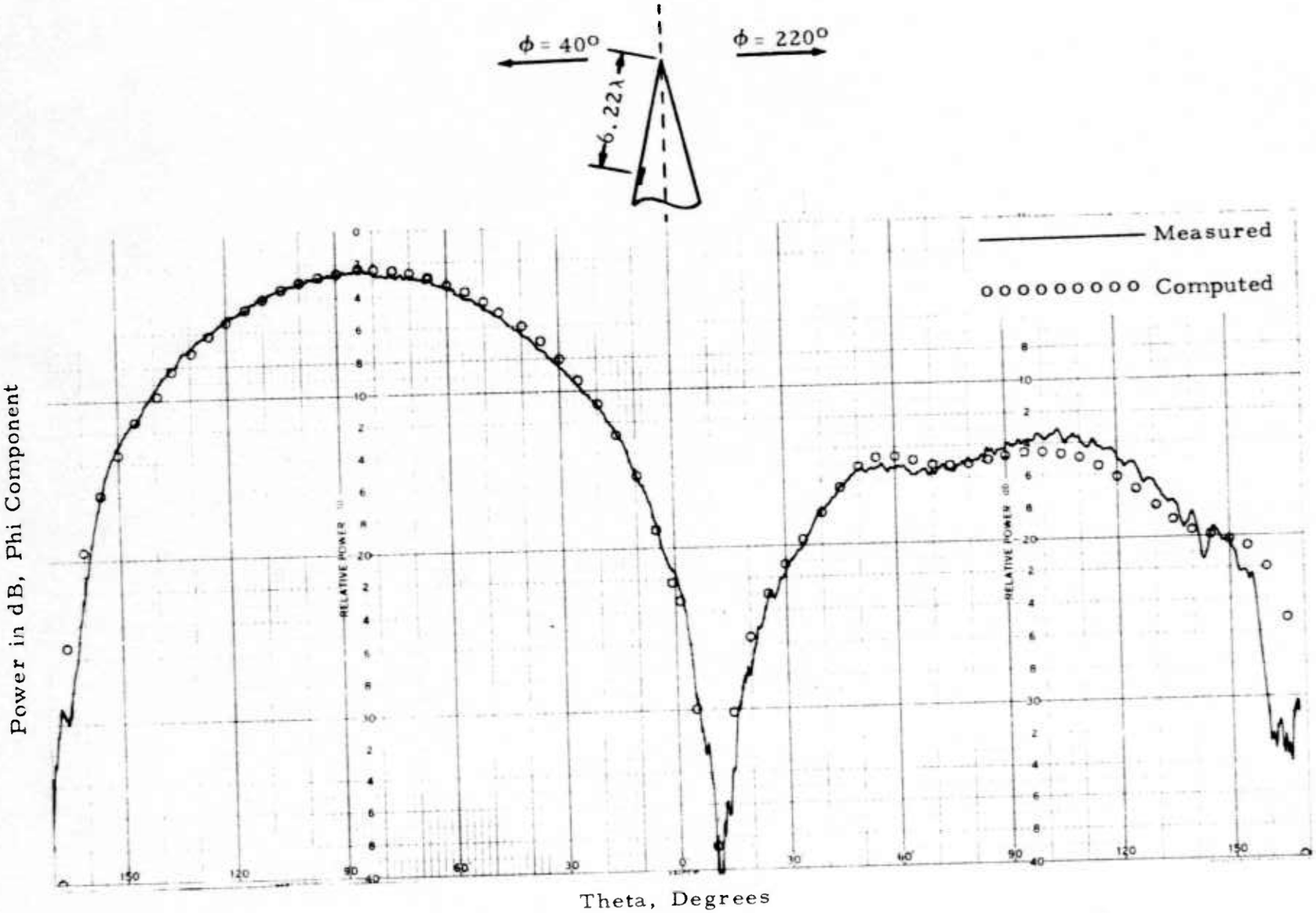

Figure 14. Measured and Computed (M = 13) ϕ-Polarized Patterns of λ/2 Radial Slot for $\phi = 40^{\circ}$, $\phi = 220^{\circ}$

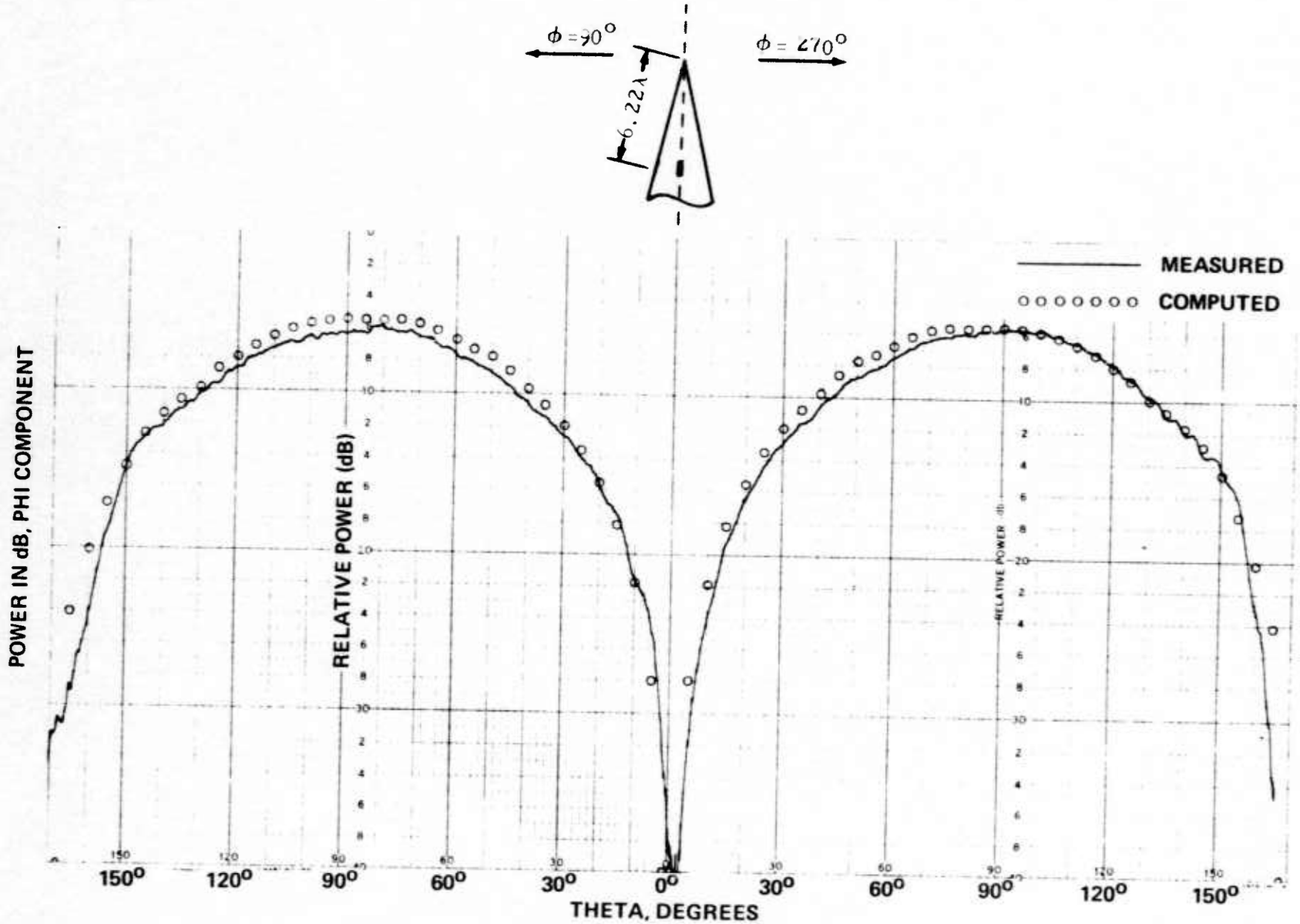

Figure 15. Measured and Computed (M = 13) ϕ-Polarized Patterns of λ/2 Radial Slot for $\phi = 90^{\circ}$, $\phi = 270^{\circ}$

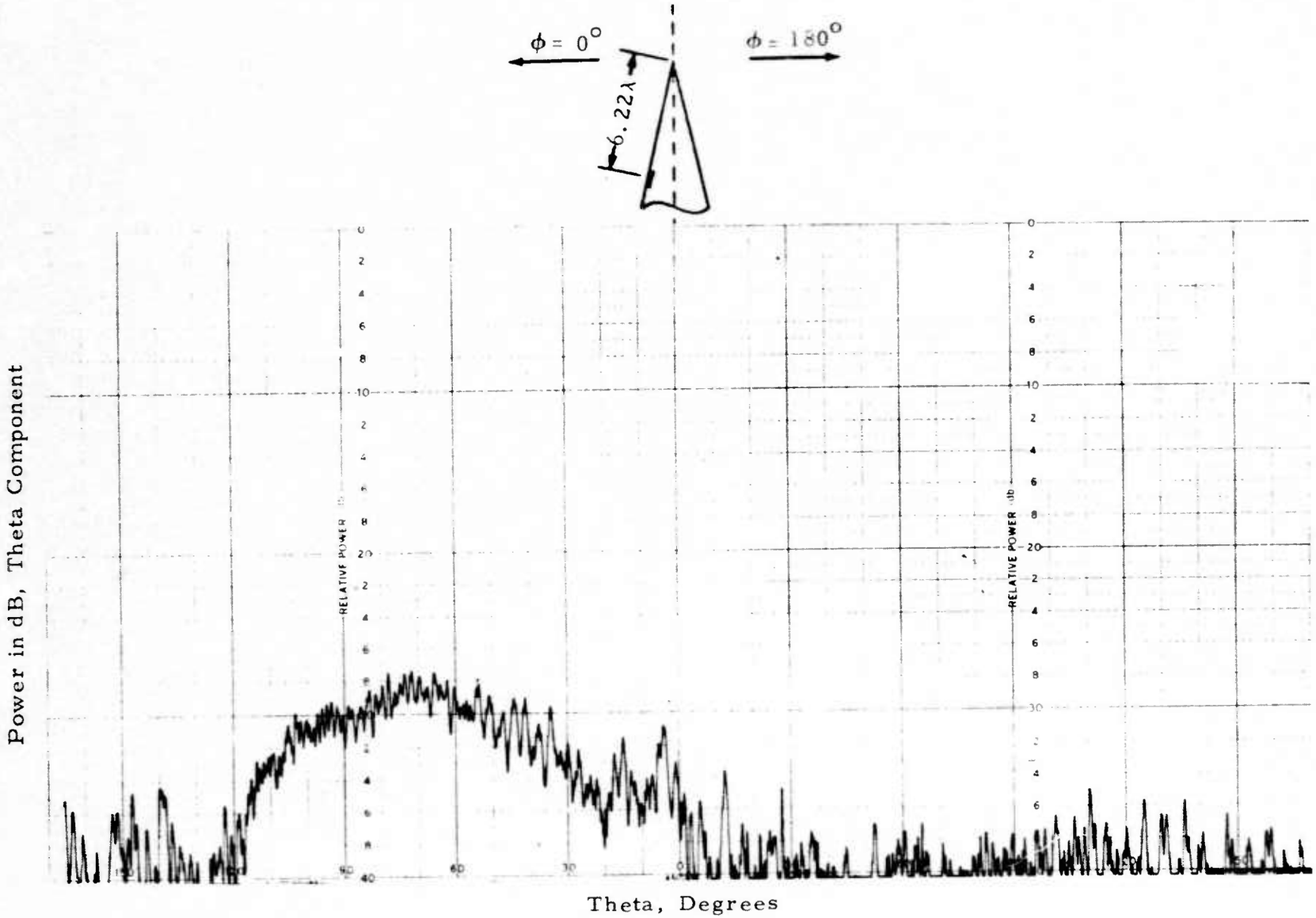

Figure 16. Measured θ-Polarized Patterns of λ/2 Radial Slot for $\phi = 0^\circ$, $\phi = 180^\circ$

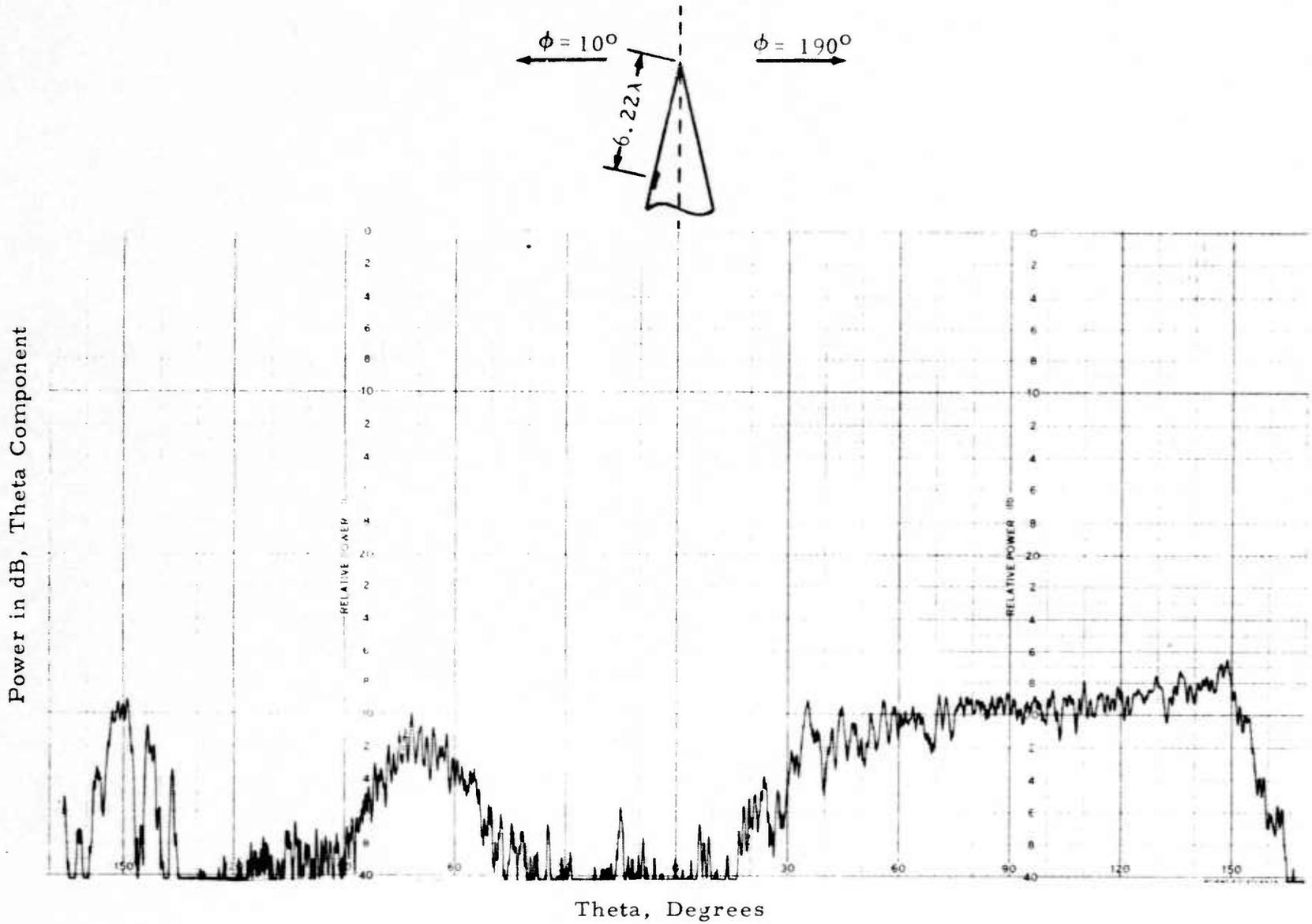

Figure 17. Measured θ-Polarized Patterns of λ/2 Radial Slot for $\phi = 10^o$, $\phi = 190^o$

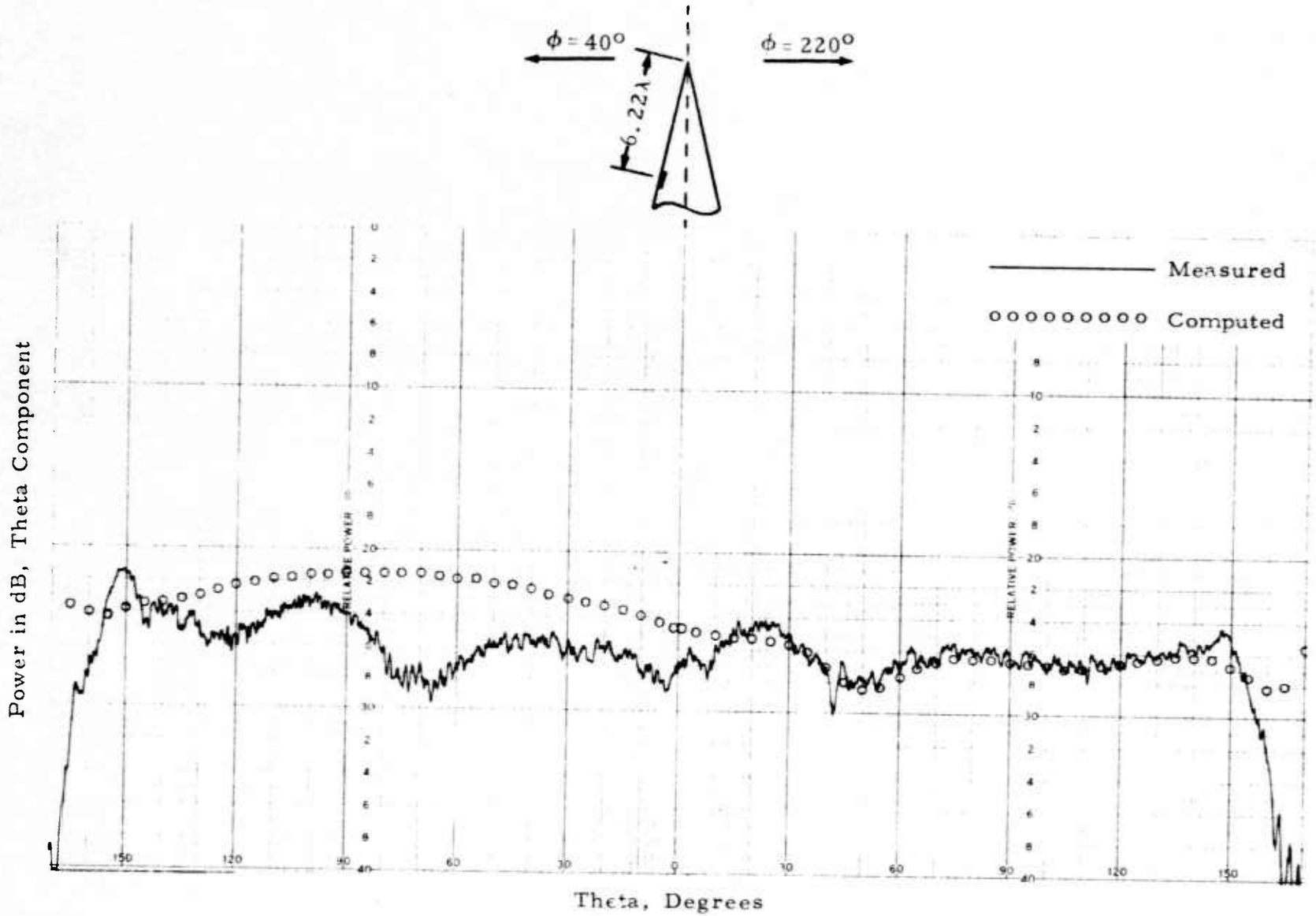

Figure 18. Measured and Computed (M = 13) θ-Polarized Patterns of λ/2 Radial Slot for $\phi = 40^{\circ}$, $\phi = 220^{\circ}$

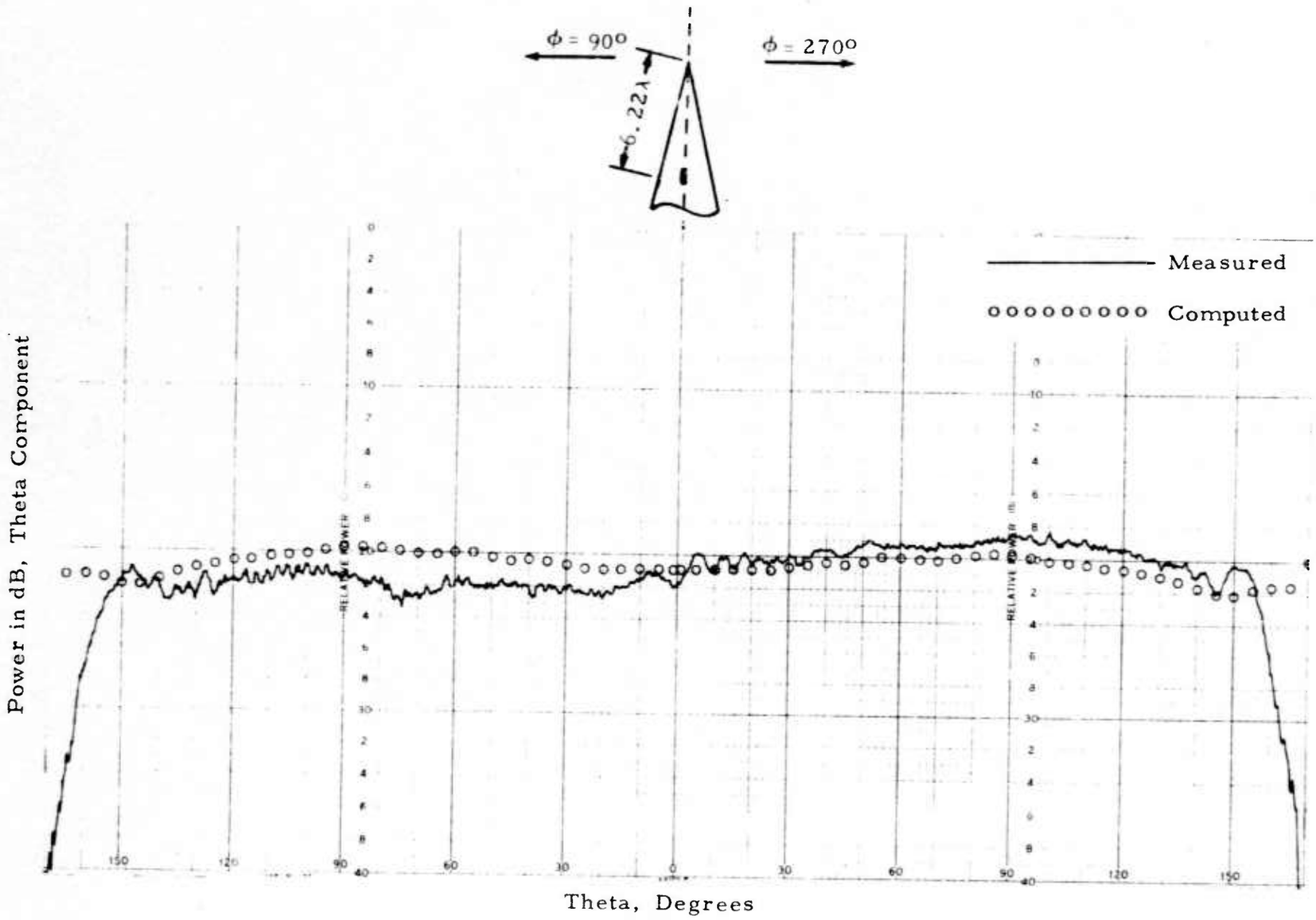

Figure 19. Measured and Computed (M = 13) θ-Polarized Patterns of λ/2 Radial Slot for $\phi = 90^{\circ}$, $\phi = 270^{\circ}$

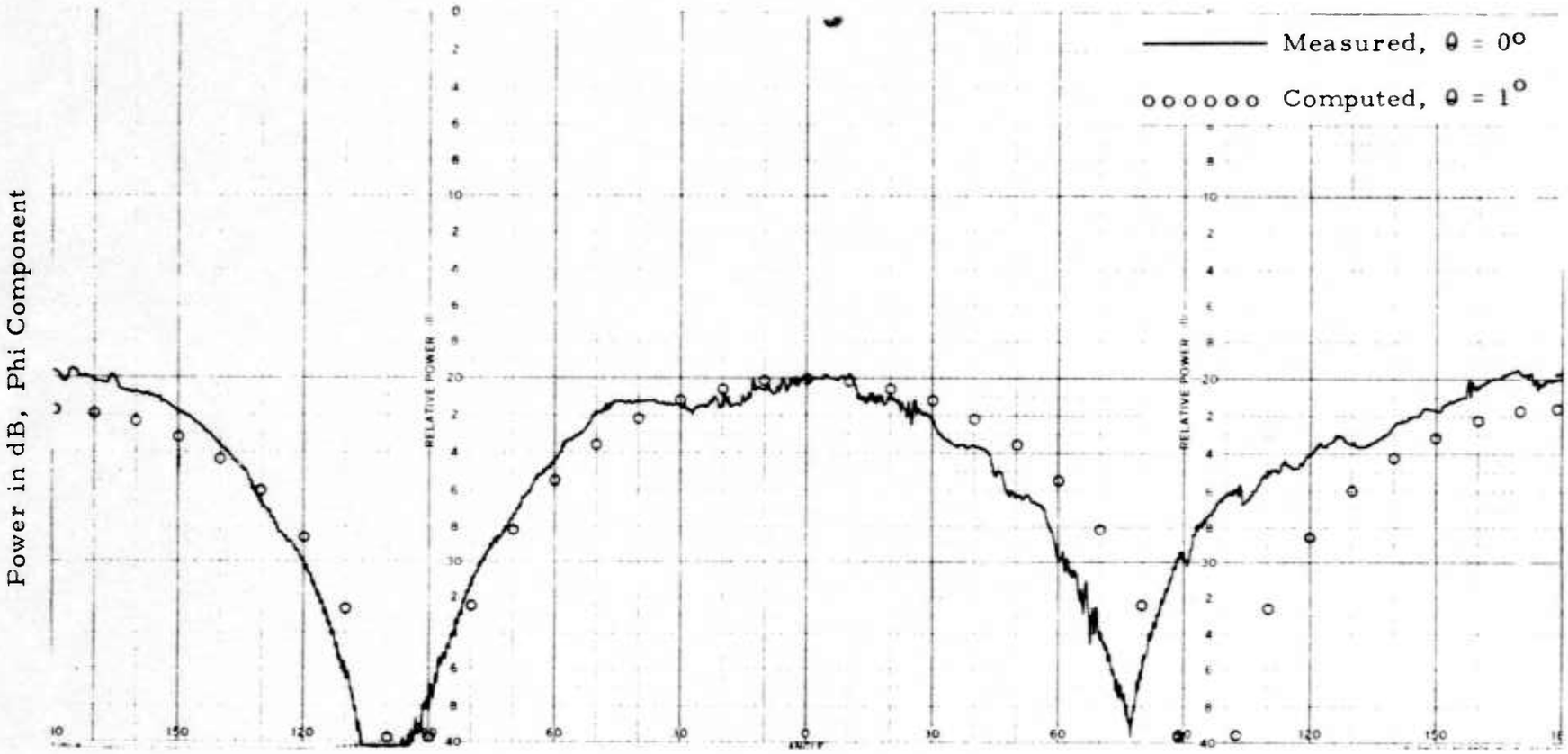

Figure 20. Measured and Computed (M = 13) ϕ-Polarized Patterns of λ/2 Radial Slot for θ = 0°, θ = 1°

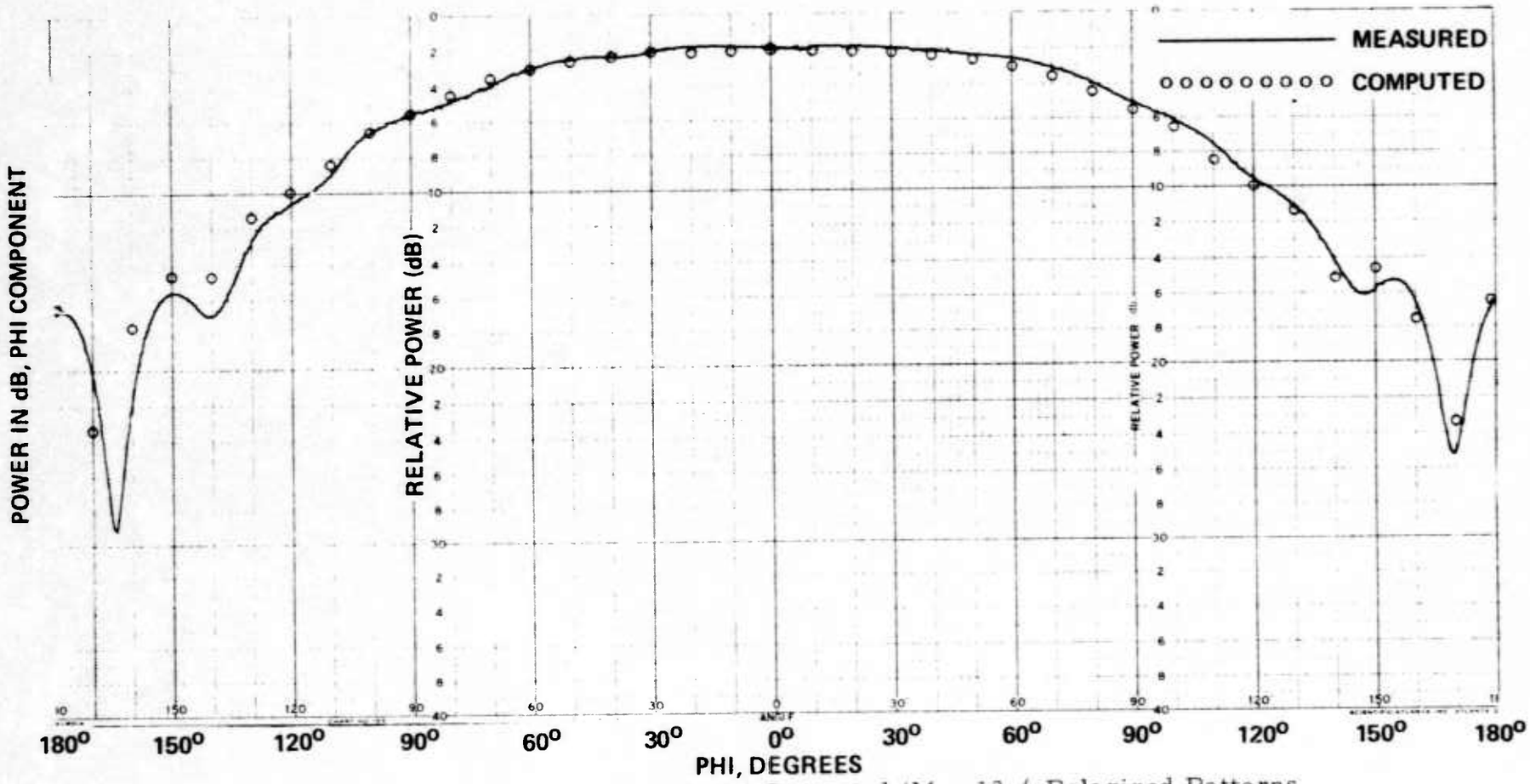

Figure 21. Measured and Computed (M = 13 ϕ-Polarized Patterns of $\lambda/2$ Radial Slot for $\theta = 80^{\circ}$

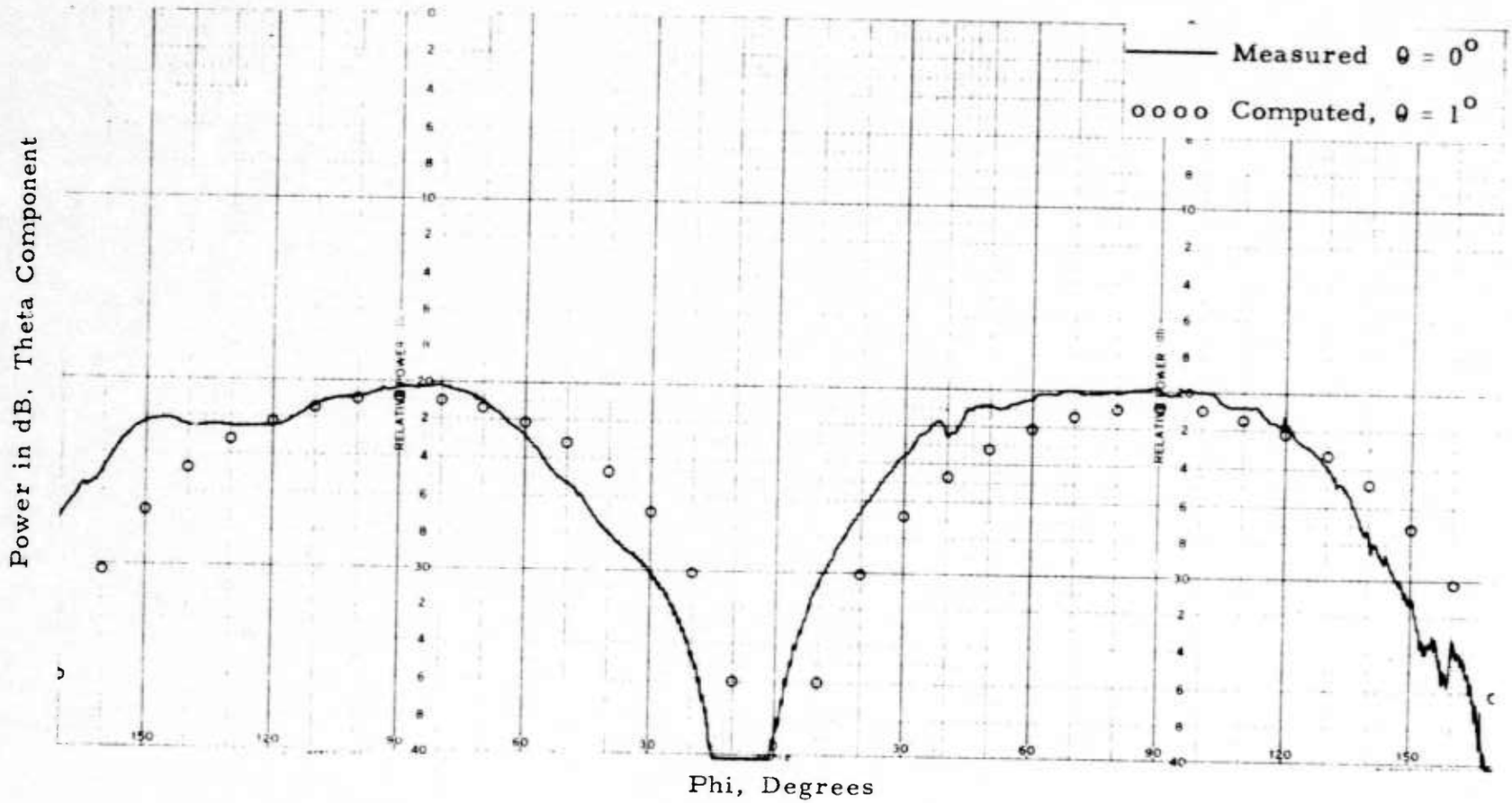

Figure 22. Measured and Computed (M = 13) θ-Polarized Patterns of λ/2 Radial Slot for θ = 0°, θ = 1°

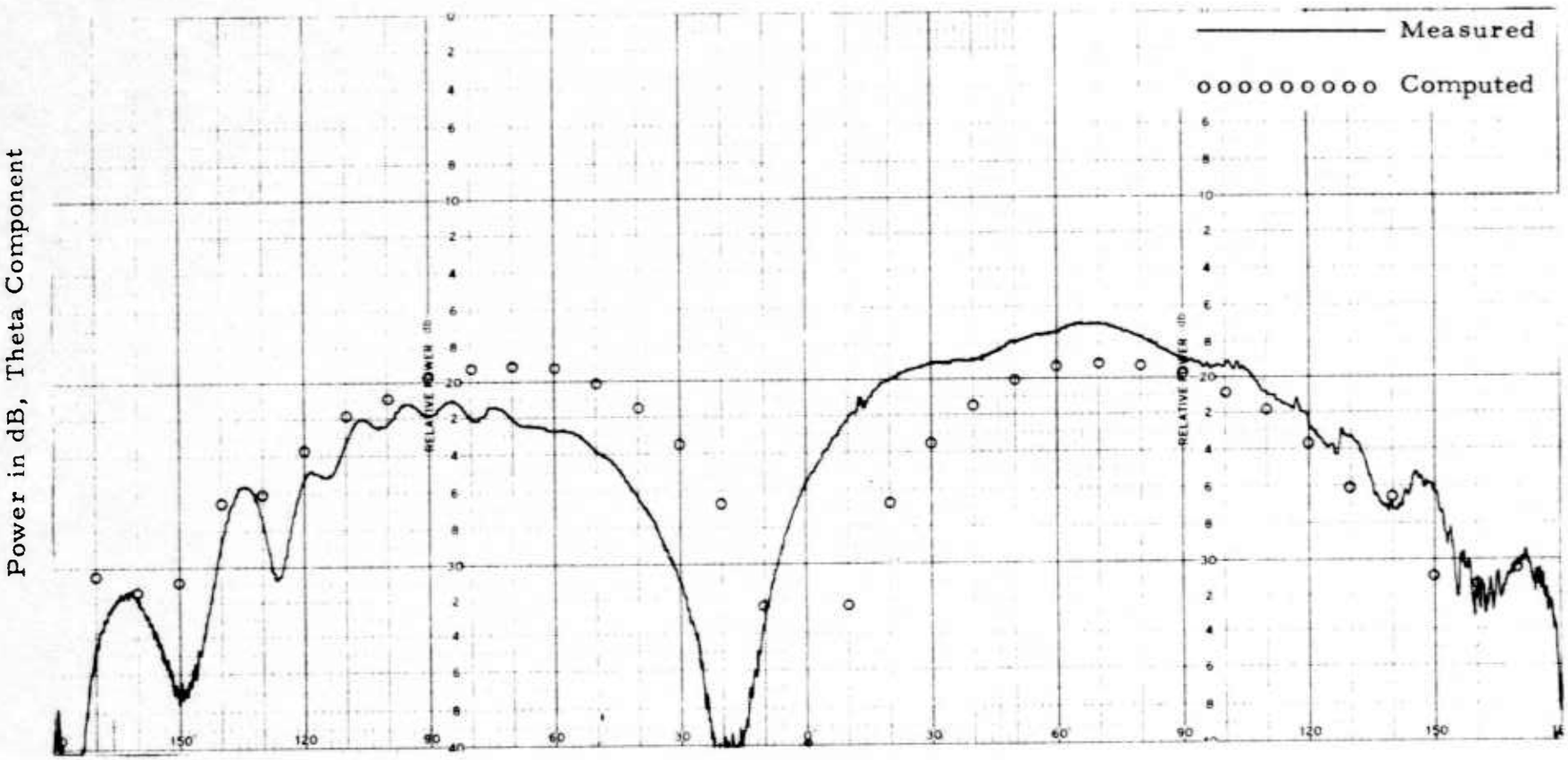

Figure 23. Measured and Computed (M = 13) θ-Polarized Patterns of λ/2 Radial Slot for $\theta = 80^{o}$

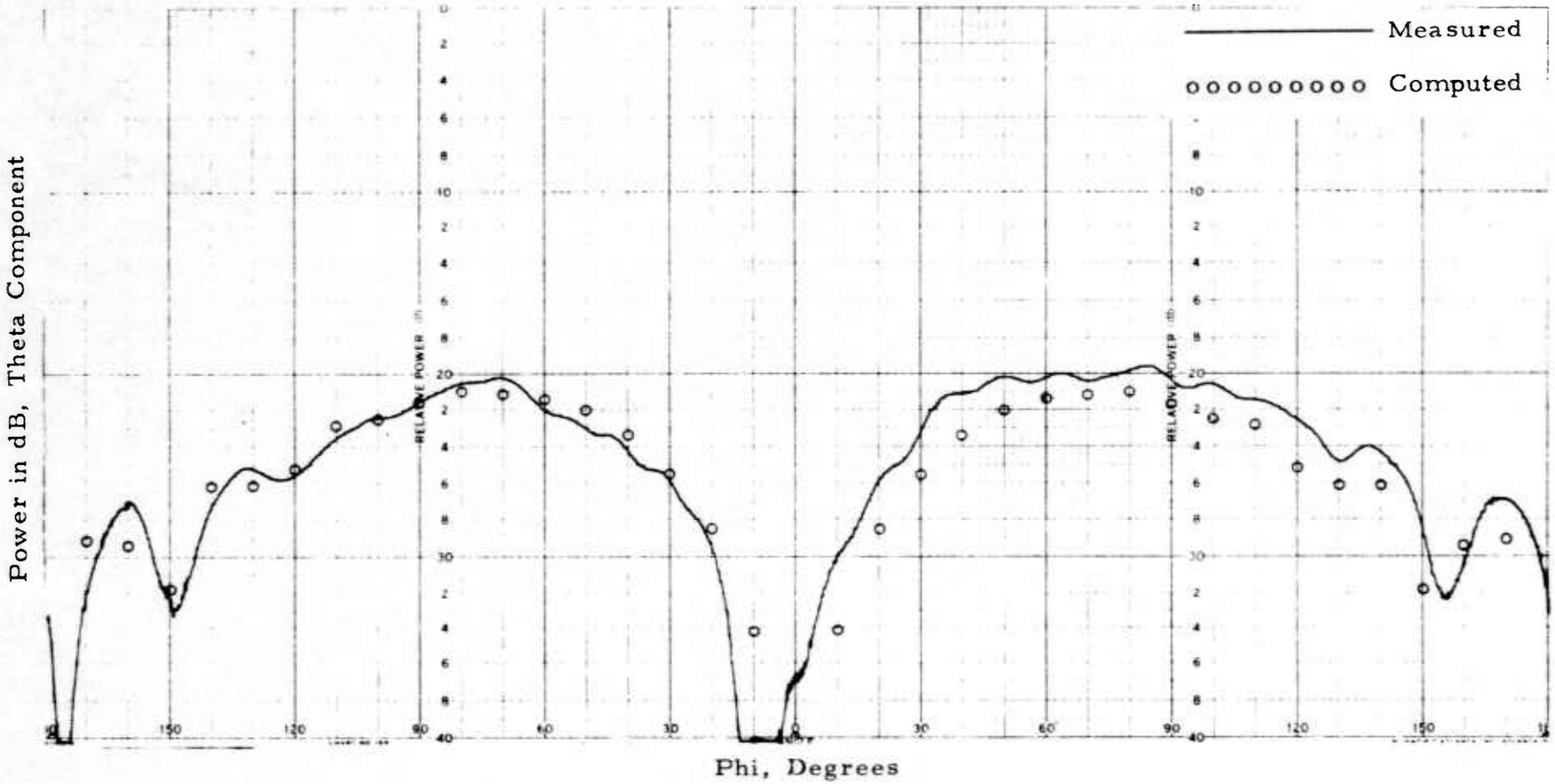

Figure 24. Measured and Computed (M = 13) θ-Polarized Patterns of λ/2 Radial Slot for θ = 140°

5. RECOMMENDATIONS FOR FURTHER INVESTIGATIONS

Computed element patterns using the normal mode series computer program have shown excellent agreement with measurements on an experimental model with both types of slots. Using the model series for the computation of exact patterns the number of modes required for convergence of the series increases as the distance of the slot location from the tip of the cone increases. Computational difficulties from accumulated round-off errors may also affect the accuracy and limit the applicability of the modal series program to element positions not too far from the cone tip.

We also have now complete expressions of the E_θ and E_ϕ radiation fields in terms of optical, transition and diffraction fields. Furthermore, it is seen that the diffraction coefficients of both components are only a function of the angular coordinates and not the location of the radiating element. The diffraction fields for any element location may then be found by the product of these diffraction coefficients and the factor containing the information of the location of the radiating element. The diffraction coefficients need be computed only once, thus eliminating the repetition of lengthy computations. The optical and transition portions of the fields, on the other hand, are given in terms of functions that are more suitable for numerical computation than the modal series expressions.

In order to utilize effectively the results of the above approximate approach for computation of radiation patterns, the expressions of both polarizations must first be programmed for use by the digital computer. The new program should be built in "blocks" as much as possible, so as

to utilize certain existing computing routines but more importantly to facilitate the integration with the modal series computer program. Such an integration of the two computer programs will be necessary since the approximate expressions, by their nature, fail to yield satisfactory results in the regions near the cone axis. Also, unlike the modal series, the asymptotic approach cannot be properly applied to radiating elements near the tip of the cone. Thus, the combination of the two programs will tend to complement one another.

Once the newly developed computer programer is tested for general accuracy and proper behavior in critical regions, it will provide the means for computing radiation patterns of both polarizations from slots on a cone. The testing should involve computation of patterns for identical slot locations that were computed by the modal series and verified by measurements. In addition to the above numerical analysis, the implications of the limiting process discussed in Section 2 should be investigated further.

The analysis technique outlined above would allow the computation of patterns to verify the equivalence principle pattern synthesis technique. Additionally, the technique could be easily extended to analyze mutual coupling and impedance of radiators on a cone from a rigorous approach and provide a check on the results obtained by the geometrical theory of diffraction.

REFERENCES

1. Abramowitz, A. and I. A. Stegun, Handbook of Mathematical Functions, National Bureau of Standards (Applied Mathematics Series 55), Washington, D. C. 1964, P. 302.

2. Bargeliotes, P. C., W. H. Kummer, and A. T. Villeneuve, 1974, "Dynamic Impedance Matching in Conformal Arrays," Final Report, January 1973 to January 1974, Contract N00019-73-C-0127, Hughes Aircraft Company.

3. Bargeliotes, P. C., "Pattern Synthesis of Conformal Arrays", Quarterly Report, January 1 to April 1, 1974, Contract N00019-74-C-0127, Hughes Aircraft Company.

4. Fried, B. D. and S. D. Conte, The Plasma Dispersion Function, New York: Academic Press, 1961, p. 3.

5. Pridmore-Brown, D. C. 1972, "Diffraction Coefficients for a Slot-Excited Conical Antenna", IEEE Trans. on Antennas and Propagation, Vol. AP-20, No. 1, January 1972, pp. 40-49.

6. Pridmore-Brown, D. C., 1973, "The Transition Field on the Surface of a Slot-Excited Conical Antenna", IEEE Trans. on Antennas and Propagation, Vol. AP-21, No. 6, November 1973, pp. 889-890.

7. Whittaker, E. T. and G. N. Watson, A Course of Mathmatical Analysis, New York: The Macmillan Company, 1944, pp. 155-156.

APPENDIX A

EVALUATION OF CONTOUR INTEGRALS

In the evaluation of the first-order integrals we are confronted with integrals of the following form.

$$I = \int_{C'_\gamma} e^{ika\cos\gamma} \ln\frac{\alpha}{\alpha-\gamma}\, d\gamma \qquad \text{(A-1)}$$

In this expression C'_γ is the deformed contour (Figure A-1) passing through the saddle point $\gamma = 0$. In addition, when evaluating the contour integral of Eq. 3.8 for small α, the following integral occurs.

$$I^B = \int_{C'_\gamma} e^{ika\cos\gamma} e^{i\gamma} \ln\frac{\alpha}{\alpha-\gamma}\, d\gamma \qquad \text{(A-2)}$$

The first integral may be obtained as a special case of the second so that only the second integral will be discussed here. When $\alpha>0$ the deformed contour must include a section along the branch cut. When $\alpha<0$ the branch cut lies entirely below the deformed contour and there is no integration along the branch cut. When $\alpha>0$ the path may be subdivided into three parts as illustrated in Figure A-2. The integral may then be written as follows:

$$\int_{C'_\gamma} e^{i(ka\cos\gamma+\gamma)} \ln\left(\frac{\alpha}{\alpha-\gamma}\right) d\gamma = \int_{C_{\gamma 1}} + \int_{Br} + \int_{C_{\gamma 2}} \qquad \text{(A-3)}$$

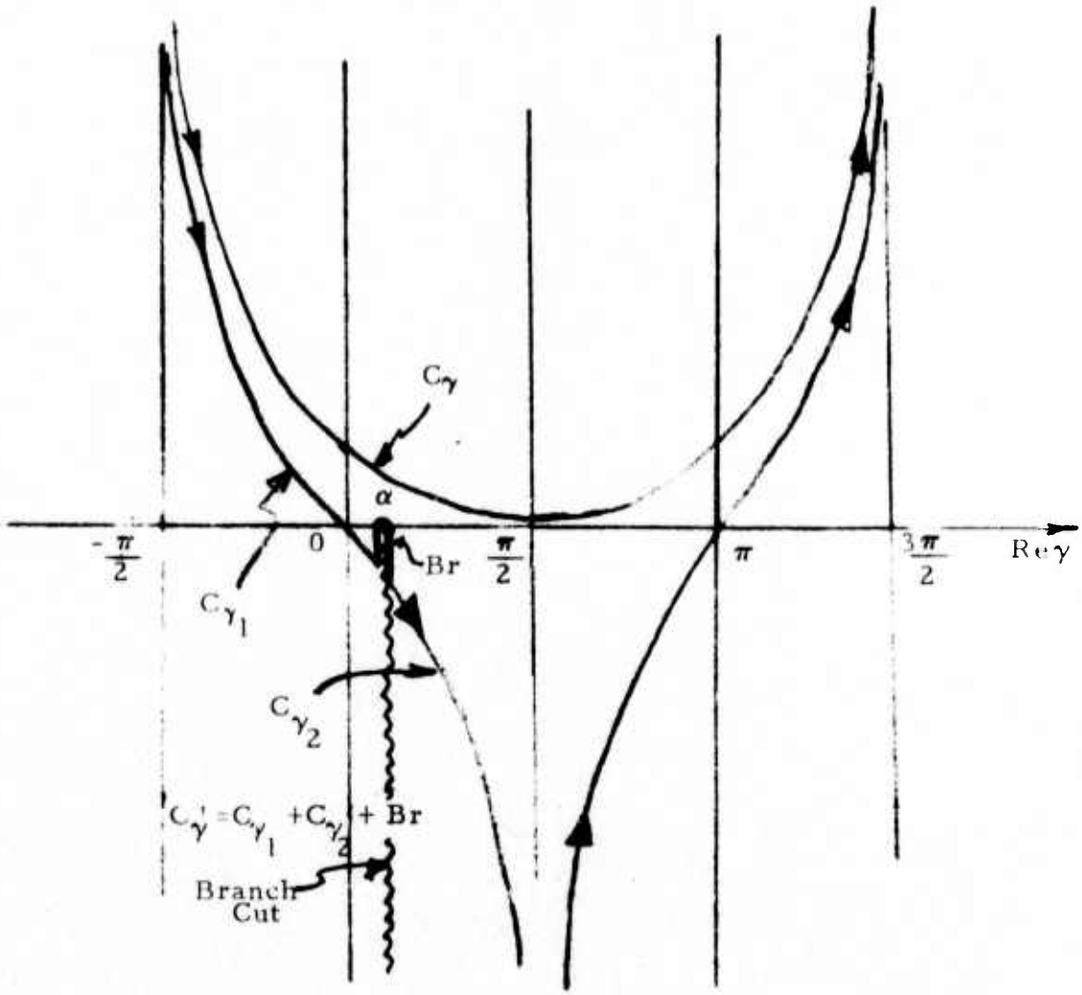

Figure A-1, Contours of Integration

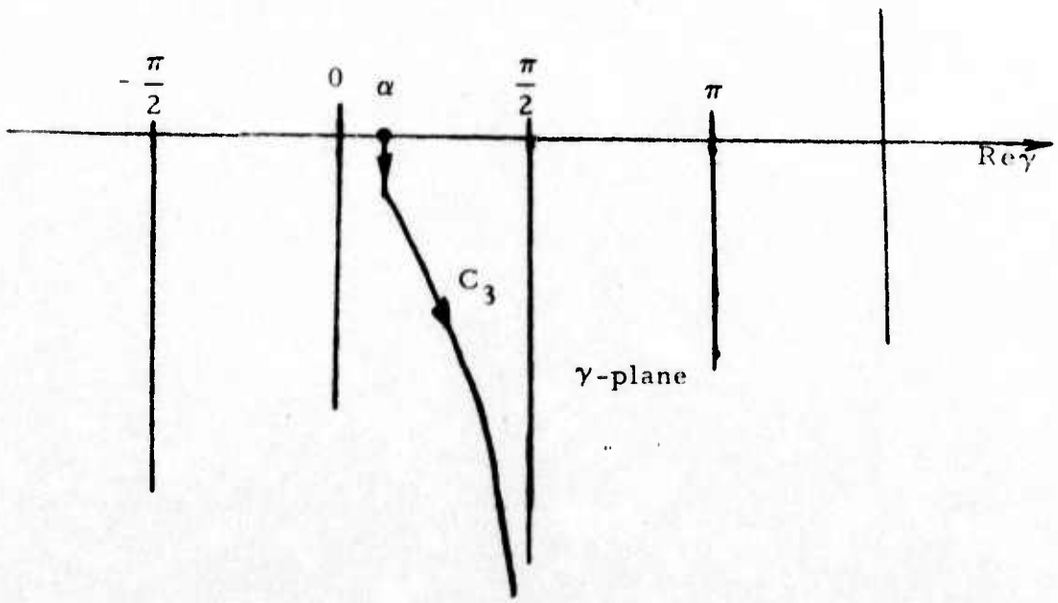

Figure A-2. Contour C_3

Along $C_{\gamma 2}$ the logarithm of $\alpha-\gamma$ differs by $-i2\pi$ from the value it would have have if there were no branch cut. Consequently, the integrals along $C_{\gamma 1}$ and $C_{\gamma 2}$ can be treated as an integral taken along both curves as though there were no branch cut plus an integral along $C_{\gamma 2}$. The deformed contour integral may now be written in the following form.

$$\int_{C_\gamma'} e^{i(ka\cos\gamma+\gamma)} \ln\left(\frac{\alpha}{\alpha-\gamma}\right)d\gamma = \int_{C_{\gamma 1}+C_{\gamma 2}} e^{i(ka\cos\gamma+\gamma)} \mathrm{Ln}\left(\frac{\alpha}{\alpha-\gamma}\right)d\gamma \tag{A-4}$$

$$+ 2\pi i \int_{C_{\gamma 2}} e^{i(ka\cos\gamma+\gamma)} d\gamma + \int_{Br} e^{i(ka\cos\gamma+\gamma)} \ln\left(\frac{\alpha}{\alpha-\gamma}\right)d\gamma$$

where arg $\mathrm{Ln}(\alpha-\gamma)$ is restricted between $-\pi$ and π.

The integral over the branch cut is obtained as follows:

$$I_{Br} = \int_{\gamma 1}^{\alpha} e^{i(ka\cos\gamma+\gamma)} \mathrm{Ln}\left(\frac{\alpha}{\alpha-\gamma}\right)d\gamma + \int_{\alpha}^{\gamma_1} e^{i(ka\cos\gamma+\gamma)} \mathrm{Ln}\left(\frac{\alpha}{\alpha-\gamma}\right)d\gamma$$
$$+ i2\pi\int_{\alpha}^{\gamma_1} e^{i(ka\cos\gamma+\gamma)} d\gamma \tag{A-5a}$$

$$I_{Br} = i2\pi\int_{\alpha}^{\gamma_1} e^{i(ka\cos\gamma+\gamma)} d\gamma \tag{A-5b}$$

where Re $\gamma_1 = \alpha$

The deformed contour may now be written in the following form:

$$\int_{C'_\gamma} e^{i(k\,a\cos\gamma+\gamma)} \ln\left(\frac{\alpha}{\alpha-\gamma}\right)d\gamma = \int_{C_{\gamma1}+C_{\gamma2}} e^{i(k\,a\cos\gamma+\gamma)} \mathrm{Ln}\left(\frac{\alpha}{\alpha-\gamma}\right)d\gamma + i2\pi \int_{C_3} e^{i(k\,a\cos\gamma+\gamma)}\, d\gamma \tag{A-6}$$

where C_3 is a contour from α vertically to $C_{\gamma2}$ and then along $C_{\gamma2}$ as shown in Figure A-2 . Since, as $\mathrm{Im}\,\gamma \to -\infty$, $e^{i\,ka\cos\gamma}$ approaches zero, for Re γ between 0 and $\frac{\pi}{2}$, the contour C_3 may be deformed to coincide with the branch cut down to $\mathrm{Im}\,\gamma \to -\infty$. Then the total deformed contour integral has the following form

$$\int_{C'_\gamma} e^{i(k\,a\cos\gamma+\gamma)} \ln\left(\frac{\alpha}{\alpha-\gamma}\right)d\gamma = \int_{C_{\gamma1}+C_{\gamma2}} e^{i[k\,a\cos\gamma+\gamma]} \mathrm{Ln}\left(\frac{\alpha}{\alpha-\gamma}\right)d\gamma + i2\pi \int_{Br_\infty} e^{i(k\,a\cos\gamma+\gamma)}\, d\gamma \tag{A-7}$$

where the subscript Br_∞ indicates a vertical path along the branch cut from α to $\alpha - i\infty$.

The branch cut integral, denoted by $I^{(1)}_{Br\phi}$, may be obtained as follows.

Let a new variable y be defined by the following relation:

$$\gamma = \alpha - i\,y \tag{A-8}$$

Then I_{Br} takes on the following form:

$$I^{(1)}_{Br\phi}(\alpha) = 2\pi \int_0^\infty e^{ika\cos\gamma} e^{i\gamma} dy. \qquad \text{(A-9)}$$

where $\gamma = (\alpha - iy)$.

On using the relationships $\cos(\alpha - iy) = \cos\alpha\cosh y + i \sin\alpha \sinh y$

$\sinh y \approx y$

$\cosh y = 1 + y^2/2$, the following expression results:

$$I^{(1)}_{Br\phi}(\alpha) = 2\pi\, e^{i(ka\cos\alpha + \alpha)} \int_0^\infty e^{i\frac{ka}{2}\cos\alpha\,[y^2 + i\,2\tan\alpha' y]}\, dy \qquad \text{(A-10)}$$

where

$$\tan\alpha' = \tan\alpha - \frac{1}{ka\cos\alpha} ,$$

which on completing the square in the exponential becomes

$$I^{(1)}_{Br\phi}(\alpha) = 2\pi\, e^{i(ka\cos\alpha + \alpha + \frac{ka}{2}\cos\alpha\tan^2\alpha')} \cdot \int_0^\infty e^{\frac{ika\cos\alpha}{2}[y + i\tan\alpha']^2} dy . \qquad \text{(A-11)}$$

The integral in (A-11) can be put into the form of a complementary error function integral by the following transformation:

$$-t^2 = i\frac{ka}{2}\cos\alpha[y + i\tan\alpha']^2$$

$$t = \sqrt{\frac{ka\cos\alpha}{2i}}[y + i\tan\alpha']$$

$$dt = \sqrt{\frac{ka\cos\alpha}{2i}}\,dy$$

giving

$$\int_0^\infty = \sqrt{\frac{2i}{ka\cos\alpha}} \int_{\sqrt{\frac{ika\cos\alpha'}{2}}\tan\alpha'}^{\infty} e^{-t^2}\,dt$$

and

$$I^{(1)}_{Br\phi}(\alpha) = \pi i e^{i(ka\cos\alpha + \alpha + \frac{ka}{2}\cos\alpha\tan^2\alpha' - \frac{\pi}{4})} \cdot \sqrt{\frac{2\pi}{ka\cos\alpha}}\,\operatorname{erfc}\left(\sqrt{\frac{ika\cos\alpha}{2}}\tan\alpha'\right) \qquad \text{(A-12)}$$

Only the integral over $C_{\gamma_1} + C_{\gamma_2}$ remains to be evaluated. Let γ' be the real part of γ and let γ'' be the imaginary part of γ. Then, on $C_{\gamma 1} + C_{\gamma 2}$

$$\sinh \gamma'' = - \tan \gamma'$$

To perform the evaluation the following substitution is made

$$v = \sin \gamma' \; / \; (\cos \gamma')^{1/2}$$

Then on $C_{\gamma 1} + C_{\gamma 2}$ the following relationships hold

$$\gamma = \sin^{-1}\left(v\left[\frac{\sqrt{v^4+4}\,-v^2}{2}\right]^{1/2}\right) - i \sinh^{-1}\left(v\left[\frac{2}{\sqrt{v^4+4}\,-v^2}\right]^{1/2}\right) \qquad \text{(A-13a)}$$

$$d\gamma = \left(1 - \frac{i\,2}{\sqrt{v^4+4}\,-v^2}\right) \frac{4\left(\frac{\sqrt{v^4+4}\,-v^2}{2}\right)^{3/2}}{\left(v^4 + 4 - v^2\sqrt{v^4+4}\right)}\, dv \qquad \text{(A-13b)}$$

$$e^{ika\cos\gamma} = e^{ika}\, e^{-kav^2} \qquad \text{(A-13c)}$$

If ka is large then $e^{-ka\ v^2}$ is very small except when v is near zero.

Then Eq. (A-13a and b) reduce to

$$\gamma \simeq e^{-i\frac{\pi}{4}}\sqrt{2}\,v$$

$$d\gamma \simeq e^{-i\frac{\pi}{4}}\sqrt{2}\,dv$$

If the additional substitutions

$$v = \frac{x}{\sqrt{ka}}$$

$$\alpha = e^{-i\frac{\pi}{4}}\sqrt{\frac{2}{ka}}\,w \equiv \sqrt{\frac{\pi}{ka}}\,u \qquad \text{(A-14)}$$

are used, the following expression results

$$\int e^{i(k\,a\cos\gamma+\gamma)}\,\mathrm{Ln}\left(\frac{\alpha}{\alpha-\gamma}\right)\,d\gamma$$

$$C_{\gamma 1}+C_{\gamma 2} = \sqrt{\frac{2\pi}{ka}}\,e^{i\left[ka-ib^2-\frac{\pi}{4}\right]}\,\frac{1}{\sqrt{\pi}}\int_{-\infty}^{\infty} e^{-(x-ib)^2}\,\mathrm{Ln}\left(\frac{w}{w-x}\right)dx \qquad \text{(A-15)}$$

where $b \equiv \dfrac{e^{-i\frac{\pi}{4}}}{\sqrt{2ka}}$

Let $U_\phi(u)$ be defined as follows:

$$U_\phi(u) = -\frac{1}{\sqrt{\pi}} \int_{-\infty}^{\infty} e^{-(x-ib)^2} \operatorname{Ln}\left(\frac{w}{w-x}\right) dx \qquad \text{(A-16a)}$$

$$U_\phi(u) = \frac{1}{\sqrt{\pi}} \int_{-\infty}^{\infty} e^{-(x-ib)^2} \operatorname{Ln}(w-x) - \operatorname{Ln}(w) \qquad \text{(A-16b)}$$

When $\alpha<0$ the deformed contour does not deviate about a branch cut. In that case, i.e, when Im $w < 0$ only $U_\phi(u)$ contributes. It is necessary, therefore, to determine methods for evaluating $U_\phi(u)$. Because of characteristics of the logarithm, different series expansions must be used for w in the upper half of the complex plane and for w in the lower half of the complex plane. There will be a discontinuity as w crosses the real axis. To determine the various expansions consider the integral portion of Eq. (A-16b).

$$F_b(w) = \frac{1}{\sqrt{\pi}} \int_{-\infty}^{\infty} e^{-(x-ib)^2} \operatorname{Ln}(w-x)dx \qquad \text{(A-17)}$$

This function is analytic in the upper half-plane and in the lower half-plane. The upper half-plane will be considered first. If Im(w) is greater than zero $F_b(w)$ is differentiable and it is possible to write the following expression

$$F_b(w) = F_b(i\varepsilon) + \int_{i\varepsilon}^{w} F_b'(y)dy \qquad \text{(A-18)}$$

where ε is a positive real number and the prime denotes differentiation with respect to w. The term $F_b'(w)$ is given by the following expression:

$$F_b'(w) = -\frac{1}{\sqrt{\pi}} \int_{-\infty}^{\infty} \frac{e^{-(x-ib)^2}}{x-w} dx \qquad \text{Im } w > 0 \qquad \text{(A-19)}$$

For w in the upper half-plane the following expression is valid.

$$\frac{1}{x-w} = i \int_{0}^{\infty} e^{-i(x-w)y} dy \qquad \text{Im } w > 0 \qquad \text{(A-20)}$$

On substituting this expression into Eq. (A-19), reversing the order of integration, the following expression is obtained:

$$F_b'(w) = -i\sqrt{\pi}\, e^{-(w-ib)^2}\left[1 - \text{erf}\,(-i[w-ib])\right] \quad \text{Im } w > 0 \qquad \text{(A-21)}$$

$$F_b'(w) = -i\sqrt{\pi}\, e^{-(w-ib)^2} + (w-ib)\sum_{n=0}^{\infty}(-1)^n \frac{(w-ib)^{2n}2^{n+1}}{1\cdot 3\cdot 5\cdots(2n+1)} \quad \text{Im } w > 0 \qquad \text{(A-22)}$$

This function is analytic in the entire complex plane including w = 0. In Eq. (A-18) the lower limit of the integral may be set equal to zero and $F_b(i\varepsilon)$ may be replaced by $F_b(i0^+)$ where

$$F_b\ (i0^+) \equiv \lim_{\varepsilon \to 0} F_b\ (i\varepsilon) \qquad \text{(A-23)}$$

This limit is given by the following expression

$$F_b\ (i0^+) = \frac{1}{\sqrt{\pi}} \int_0^\infty (e^{-(x+ib)^2} + e^{-(x-ib)^2}) \ln x\, dx + i\frac{\pi}{2}[1+\mathrm{erf}(ib)] \qquad \text{(A-24)}$$

and is obtained using the condition $-\pi < \arg \ln z < \pi$. The integral can be evaluated numerically. For such an evaluation an integration by parts is first performed to remove the logarithmic singularity. The resulting expression is as follows:

$$F(i0^+) = I(b) + i\frac{\pi}{2}[1 + \mathrm{erf}\ (ib)] \qquad \text{(A-25)}$$

where

$$I(b) = \frac{1}{\sqrt{\pi}} \int_0^\infty [e^{-(x+ib)^2} + e^{-(x-ib)^2}] \ln x\, dx$$

$$= \frac{2}{\sqrt{\pi}} \int_0^\infty [(x+ib)e^{-(x+ib)^2} + (x-ib)e^{-(x-ib)^2}]\, x(\ln x - 1)\, dx$$

On using Eq. (A-25) and integrating Eq. (A-22) the following expression for $F_b(w)$ is obtained when w is in the upper half-plane.

$$F_b(w) = I(b) + i\frac{\pi}{2}[1 - \mathrm{erf}(w-ib)] + \sum_{n=0}^{\infty} \frac{(-1)^n[(w-ib)^{2n+2} - (ib)^{2n+2}]2^n}{1\cdot 3\cdot 5\cdots(2n+1)\ (n+1)} \qquad \mathrm{Im}\ w > 0 \qquad \text{(A-26)}$$

If w is in the lower half-plane then instead of Eq. (A-20) the following relationship is used.

$$\frac{1}{x-w} = -i\int_0^{\infty} e^{i(x-w)y}\,dy \qquad \mathrm{Im}\ w < 0 \qquad \text{(A-27)}$$

If an analysis is carried through in a manner similar to the preceding one the following expression results for $F_b(w)$ in the lower half-plane.

$$F_b(w) = I(b) - i\frac{\pi}{2}[1-\mathrm{erf}(w-ib)] + \sum_{n=0}^{\infty} \frac{(-1)^n[w-ib)^{2n+1} - (ib)^{2n+2}]\ 2^n}{1\cdot 3\cdot 5\cdots(2n+1)\ (n+1)} \qquad \mathrm{Im}\ w < 0 \qquad \text{(A-28)}$$

The function $U_\phi(u)$ and $U(u)$ are then given by the following expressions

$$U_\phi(u) = F_b(w) - \ln w \qquad \text{(A-29)}$$

$$U(u) = \lim_{b\to 0} U_\phi(u) \qquad \text{(A-30)}$$

It may be shown that U(u) is an even function of u. In addition

$$\lim_{b \to 0} I(b) = -\frac{C}{2} \tag{A-31}$$

where C is Euler's constant.

$$C = 0.577215665... \tag{A-32}$$

When Im w >0 the branch cut integral must be added. When Im w< 0 there is no branch cut integral. Eqs. (A-26) and (A-28) permit computation of $U_\phi(u)$ for reasonably small values of $|w - ib|$. For large values of $|w - ib|$ an asymptotic expansion is desired. Such an expansion can be obtained directly from the integral expression. To accomplish this expansion rewrite Eq. (A-16b) in the following form:

$$U_\phi(u) = \frac{1}{\sqrt{\pi}} \int_{-\infty}^{\infty} e^{-(x-ib)^2} \mathrm{Ln}\big((w-ib) - (x-ib)\big)\, dx - \mathrm{Ln}\, w \tag{A-33}$$

As long as w - ib is not pure imaginary, then as $|w-ib|$ increases without limit, the main contribution to the contour integral is from $U_\phi(u)$. In turn, the main contribution of $U_\phi(u)$ will come from the region where Re(x-ib) is a minimum, i.e., where x=Re b<< $|w-ib|$. Then the logarithm may be expanded in powers of $\frac{x-ib}{w-ib}$ and the resulting expression may be integrated term-by-term. This process leads to the following expression:

$$U_\phi(u) \sim \mathrm{Ln}\,(w-ib) - \mathrm{Ln}\,(w) - \sum_{n=1} \frac{1}{n(w-ib)^n} \frac{1}{\sqrt{\pi}} \int_{-\infty}^{\infty} (x-ib)^n e^{-(x-ib)^2} dx \tag{A-34}$$

$$\sim \mathrm{Ln}\,(w-ib) - \mathrm{Ln}(w) - \sum_{n=1} \frac{1\cdot 3\cdot \cdots \cdot (2n-1)}{2n(w-ib)^{2n} 2^n} \qquad |w-ib| \to \infty$$

When b = 0 the following expansion for U(u) results:

$$U(u) \sim - \sum_{n=1} \frac{1 \cdot 3 \cdots (2n-1)}{2n\, w^{2n} 2^n} \qquad |w| \to \infty \tag{A-35}$$

The total integral may then be written as follows:

$$\int_{C'_\gamma} e^{i\,[ka \cos \gamma + i\gamma]} \ln \frac{\alpha}{\alpha - \gamma}\, d\gamma$$

$$= I^{(1)}_{BR}\ (\alpha)\ H\ (\alpha) - \sqrt{\frac{2\pi}{ka}}\ e^{i(ka - ib^2 - \frac{\pi}{4})}\ U_\phi(u) \tag{A-36}$$

For large values of ka the b^2 in the exponent may be omitted.

An alternative derivation of the contour integral in which the branch cut is taken from α along the negative real axis results in a slightly different expansion for the integral valid for α sufficiently small that $\cos \alpha \approx 1 - \alpha^2/2$. The expansion is as follows:

$$\int_{C'_\gamma} e^{i(ka \cos \gamma + \gamma)} \ln \left(\frac{\alpha}{\alpha - \gamma}\right) d\gamma$$

$$\sim - \sqrt{\frac{2\pi}{ka}}\ e^{i(ka - ib^2 - \frac{\pi}{4})} \left[I(b) - i\,\frac{\pi}{2}\,[1 - \operatorname{erf}\,(w - ib)] \right. \tag{A-37}$$

$$\left. + \sum_{n=0}^{\infty} \frac{(-1)^n\,[(w-ib)^{2n+2} - (ib)^{2n+2}]\ 2^n}{1 \cdot 3 \cdot 5 \cdots (2n+1)\ (n+1)} - \ln w \right] \qquad w \neq 0$$

This expression is valid for Im (w) both positive and negative and agrees with the previous results as $w \to 0$.

When α is near the saddle point at $\gamma=\pi$ then the integral of interest is as follows.

$$I = \int_{C'_\gamma} e^{i[\,ka\cos\gamma + \gamma]} \ln\left(\frac{\alpha-\pi}{\alpha-\gamma}\right) d\gamma \qquad \text{(A-38)}$$

where C_γ passes upward through the saddle point at π. This integral leads to the following integrals

$$I = 2\pi \int_{-\infty}^{\infty} e^{i[ka\ \cos\alpha\cosh y + i\sin\alpha\sinh y]}\, e^{i(\alpha - iy)}\, dy\, H(\pi-\alpha)$$

$$+ \sqrt{\frac{2\pi}{ka}}\ e^{-i\left(ka - ib^{*2} - \frac{\pi}{4}\right)} \left[-\frac{1}{\sqrt{\pi}} \int_{-\infty}^{\infty} e^{-(x+ib^*)} \operatorname{Ln}\left(\frac{\bar{w}^*}{\bar{w}^*-x}\right) dx\right] \qquad \text{(A-39)}$$

$$= -\,I^{(1)*}_{BR_\phi}(\bar{\alpha})\, H(\bar{\alpha}) - \sqrt{\frac{2\pi}{ka}}\ e^{-i\left(ka - ib^{*2} - \frac{\pi}{4}\right)}\, U^*_\phi(\bar{u})$$

where

$$\bar{\alpha} \equiv \pi - \alpha$$

$$\bar{u} \equiv \sqrt{\frac{ka}{\pi}}\ (\pi - \alpha)$$

$$\bar{w} \equiv \sqrt{\frac{ka}{2}}\ e^{i\frac{\pi}{4}}\ (\pi - \alpha)$$

APPENDIX B

EXPANSION OF $B'_{1n}(\theta, \theta_o)$, $B_{in}(\theta, \theta_o)$, $B'_{2n}(\theta, \theta_o)$

Expansion of $B'_{1n}(\theta, \theta_o)$:

We begin with the asymptotic representation of Legendre functions:

$$P^{-m}_{\nu-\frac{1}{2}}(\cos\theta) = \left(\frac{2}{\pi \sin\theta}\right)^{1/2} \nu^{-m-\frac{1}{2}} \left\{ \sin\psi - \frac{1-4m^2}{8\nu} \cot\theta \cos\psi \right\} \qquad \text{(B-1)}$$

where

$$\psi = \nu\theta + (1-2m)\frac{\pi}{4}$$

Equation (13) then becomes

$$B'_{in}(\theta,\theta_o) = \left(\frac{\sin\theta_o}{\sin\theta}\right)^{\frac{1}{2}} \frac{1}{\theta_o} \left\{ \nu_n \frac{\cos\psi}{\cos\psi_o} - \frac{3+4m^2}{8} \cot\theta \frac{\sin\psi}{\cos\psi_o} \right\} \qquad \text{(B-2)}$$

First-order and second-order roots of $P^{-m}_{\nu-\frac{1}{2}}(\cos\theta) = 0$ are then found as follows:

First-order Roots

$$\sin\psi_o = 0 \quad , \quad \psi_o^{(1)} = n\pi$$

$$\nu_n^{(0)} = \left(n - \frac{1}{4} + \frac{m}{2}\right)\frac{\pi}{\theta_o} \quad , \quad n = 1, 2, 3, \ldots \qquad \text{(B-3)}$$

Second-order Roots

$$\sin\psi_o = \frac{1-4m^2}{8\nu} \cot\theta \cos\psi_o$$

$$\tan\psi_o = \frac{1-4m^2}{8\nu_n^{(0)}} \cot\theta_o = \epsilon \qquad \text{(B-4)}$$

By taking a Taylor expansion of $\tan\psi_o$ about $\psi_o^{(1)} = n\pi$, we find

$$\nu_n^{(1)} = \nu_n^{(0)} + \frac{\epsilon}{\theta_o} \qquad \text{(B-5)}$$

The desired expansions of $\frac{\cos\psi}{\cos\psi_o}$ and $\frac{\sin\psi}{\cos\psi_o}$ which appear in $B'_{1n}(\theta, \theta_o)$ in terms of first-order and second-order roots are found by taking $\psi = \psi - \psi_o + \psi_o$. Then,

$$\psi - \psi_0 = \nu\theta + (1-2m)\frac{\pi}{4} - \nu\theta_0 - (1-2m)\frac{\pi}{4}$$

$$= \nu_n^{(0)}(\theta-\theta_0) + \epsilon\left(\frac{\theta}{\theta_0}-1\right) \qquad \text{(B-6)}$$

$$\psi_0 = n\pi + \epsilon \qquad \text{(B-7)}$$

$$\cos\psi = \cos(\psi-\psi_0)\cos\psi_0 - \sin(\psi-\psi_0)\sin\psi_0$$

$$= (-1)^n \left[\cos\nu_n^{(0)}(\theta-\theta_0) - \epsilon\frac{\theta}{\theta_0}\sin\nu_n^{(0)}\right] \qquad \text{(B-8)}$$

where we have taken $\sin\epsilon \approx \epsilon$ and $\cos\epsilon \approx 1$, since $\epsilon \to 0$.

Similarly, we find

$$\sin\psi = \sin(\psi-\psi_0)\cos\psi_0 + \cos(\psi-\psi_0)\sin\psi_0$$

$$= (-1)^n \left[\sin\nu_n^{(0)}(\theta-\theta_0) + \epsilon\frac{\theta}{\theta_0}\cos\nu_n^{(0)}(\theta-\theta_0)\right] \qquad \text{(B-9)}$$

$$\cos\psi_0 = \cos[n\pi+\epsilon] = (-1)^n \qquad \text{(B-10)}$$

With (B-8), (B-9), and (B-10) in (B-2) and the asymptotic representation of the Bessel function the terms in the residue series approach the following values in terms of the first-order and second-order roots, $\nu_n^{(0)}$ and $\nu_n^{(1)}$. Thus,

$$\frac{\mu_n}{\mu_n^2-\frac{1}{4}} B'_{1m}(\theta,\theta_0)\, j^{-\nu_n} J_{\nu_n}(ka)(2\pi ka)^{1/2} e^{-j(ka-\frac{\pi}{4})}$$

$$\approx \frac{\mu_n}{\mu_n^2-\frac{1}{4}}\left(\frac{\sin\theta_0}{\sin\theta}\right)^{\frac{1}{2}}\frac{\mu_n}{\theta_0}\left\{\cos\nu_n^{(0)}(\theta-\theta_0)\right.$$

$$\left. - \frac{1}{\nu_n^{(0)}}\eta_1 \sin\nu_n^{(0)}(\theta-\theta_0)\right\} j^{-2\nu_n} \qquad n \gg 1 \qquad \text{(B-11)}$$

But,

$$i^{-2\nu_n} = e^{-i(\nu_n^{(0)} + \frac{\epsilon}{\theta_0})\pi} \approx e^{-i\nu_n^{(0)}\pi}\left[1 - i\frac{\epsilon}{\theta_0}\pi\right]$$

$$\approx e^{-i\nu_n^{(0)}\pi}\left[1 - \frac{i}{\nu_n^{(0)}}\frac{1-4m^2}{8}\frac{\pi}{\theta_0}\cot\theta_0\right] = e^{-i\nu_n^{(0)}\pi}\left[1 - \frac{i\eta_2}{\nu_n^{(0)}}\right] \quad \text{(B-12)}$$

where

$$\eta_2 = \frac{1-4m^2}{8}\frac{\pi}{\theta_0}\cot\theta_0 \ .$$

Substituting (B-12) in (B-11) and retaining the zeroth-order and first-order terms in $1/\nu_n$, the right-hand side of (B-11) becomes

$$\frac{1}{\theta_0}\left(\frac{\sin\theta_0}{\sin\theta}\right)^{1/2}\left\{\cos\nu_n^{(0)}(\theta-\theta_0)\, e^{-i\nu_n^{(0)}\pi}\right.$$

$$\left. + \frac{\theta_0}{n\pi}\left[\eta_1 \sin\nu_n^{(0)}(\theta_0-\theta) - i\eta_2\cos\nu_n^{(0)}(\theta_0-\theta)\right] e^{-i\nu_n^{(0)}\pi}\right\} \quad \text{(B-13)}$$

$n >> 1$

The first term in the braces gives $Q_n(\theta, \theta_0)$ while the last two terms give $R_n(\theta, \theta_0)$ after replacing the coefficient $\frac{1}{\nu_n(0)}$ by $\frac{\theta_0}{n\pi}$

Expansion of $B_{1n}(\theta, \theta_0)$

On using (B-1) in (13) of Section 2, and dropping higher order terms in $1/\nu$, we find

$$B_{1n}(\theta, \theta_0) = \left(\frac{\sin\theta_0}{\sin\theta}\right)^{\frac{1}{2}} \frac{\sin\psi}{\theta_0\cos\psi_0}\cdot$$

$$\cdot\left(1 - \frac{(1-4m^2)[\cot\theta_0\cot\psi + \cot\theta_0\tan\psi_0] - 4(1+2m)\frac{\tan\psi_0}{\theta_0}}{8\nu}\right) \quad \text{(B-14)}$$

Substituting (B-9) and (B-10) for $\sin\psi$ and $\cos\psi_o$, respectively,

$$B_{1n}(\theta, \theta_o) \sim \left(\frac{\sin\theta_o}{\sin\theta}\right)^{\frac{1}{2}} \frac{1}{\theta_o}\left[\frac{\sin \nu_n^{(o)}(\theta-\theta_o)+ (4m^2-1)\cos \nu_n^{(o)}(\theta-\theta_o)}{8\,\nu_n^{(o)}}\right] \quad \text{(B-15)}$$

If we now use the asymptotic representation of the Bessel function, we can express the nth term of the residue series in terms of the first-order roots, $\nu_n^{(o)}$, resulting in

$$R_{1n\phi}(\theta, \theta_o) \approx \frac{\nu_n}{\nu_n^2 - 1/4} B_{1n}(\theta, \theta_o) i^{-\nu_n} J_{\nu_n}(ka)\,(2\pi ka)^{\frac{1}{2}}\, e^{-i\,(ka-\pi/4)}$$

$$\approx \left(\frac{\sin\theta_o}{\sin\theta}\right)^{\frac{1}{2}} \frac{\sin \nu_n^{(o)}(\theta-\theta_o)}{n\pi}\, e^{-i\,\nu_n^{(o)}\pi} \quad \text{(B-16)}$$

where $\nu_n^{(o)} \approx \frac{n\pi}{\theta_o}$ has been used in the magnitude factor. The above expression may be summed to give an approximate closed form, $R_{1\phi}(\theta, \theta_o)$, as follows:

$$R_{1\phi}(\theta,\theta_o) = \sum_{n=1}^{\infty} R_{1n\phi}(\theta, \theta_o) = \sum_{n=1}^{\infty}\left(\frac{\sin\theta_o}{\sin\theta}\right)^{\frac{1}{2}} \frac{\sin \nu_n^{(o)}(\theta-\theta_o)\, e^{-i\,\nu_n^{(o)}\pi}}{n\pi}$$

$$= -\frac{1}{2\pi i}\left(\frac{\sin\theta_o}{\sin\theta}\right)^{\frac{1}{2}} \sum_{n=1}^{\infty} \frac{1}{n}\left[e^{-i\,\nu_n^{(o)}(\pi-\theta_o+\theta)} - e^{-i\,\nu_n^{(o)}(\pi+\theta_o-\theta)}\right]$$

$$= \frac{i}{2\pi}\left(\frac{\sin\theta_o}{\sin\theta}\right)^{\frac{1}{2}} \left[g_1(\alpha, \xi) - g_1(\beta, \xi)\right] \quad \text{(B-17)}$$

with $g_1(\alpha, \xi)$, $g_2(\beta, \xi)$ defined below equation (47-c).

Expansion of $B'_{2n}(\theta, \theta_o)$

On using (B-1) in (13a) of Section (2) and dropping higher order terms in $1/\mu$, we find

$$B'_{2n}(\theta, \theta_o) = -\left(\frac{\sin\theta_o}{\sin\theta}\right)^{\frac{1}{2}} \frac{\cos\psi}{\theta_o \sin\psi_o} \cdot \left[1 - \frac{(3+4m^2)\cot\theta\tan\psi + \cot\theta_o\cot\psi_o + 8(m-\frac{1}{2})\frac{\cot\psi_o}{\theta_o}}{8\mu_n}\right] \quad \text{(B-18)}$$

We now find the first-order and second-order roots of $(\partial/\partial\theta_o) P^{-m}_{\mu-\frac{1}{2}}(\cos\theta_o) = 0$, by differentiating (B-1) and setting the result equal to zero. Thus,

$$\mu\cos\psi_o - \frac{1-4m^2\cos\psi_o}{\sin^2\theta_o\, 8\mu} - \frac{3+4m^2}{8}\cot\theta_o\sin\psi_o = 0 \quad \text{(B-19)}$$

or

$$\cot\psi_o = \epsilon \Big/ \left[1 - \frac{1-4m^2}{8\mu^2\sin^2\theta_o}\right] = \epsilon' \quad \text{(B-20)}$$

First-order root:

Setting $\epsilon = 0$, $\cot\psi_o = 0$ when $\psi_o^{(1)} = (2n+1)\frac{\pi}{2}$, giving

$$\mu_n^{(0)} = (n + \frac{1}{4} + \frac{m}{2})\frac{\pi}{\theta_o} \qquad n = 1, 2, \ldots \quad \text{(B-21)}$$

Second-order root:

By expanding $\cot \psi_o$ in a Taylor series about $\psi_o^{(1)}$, we find from (B-19)

$$\cot \psi_o^{(1)} - \csc^2 \psi_o^{(1)} \left(\psi_o^{(2)} - \psi_o^{(1)} \right) = \epsilon' \qquad \text{(B-22)}$$

and $\psi_o^{(2)} = \psi_o^{(1)} + \epsilon'$ since $\cot \psi_o^{(1)} \longrightarrow 0$. Then,

$$\mu_n^{(2)} \theta_o + (1-2m) \frac{\pi}{4} = (2n+1) \frac{\pi}{2} + \epsilon'$$

$$\text{or} \quad \mu_n^{(2)} = \mu_n^{(0)} + \frac{\epsilon'}{\theta_o} \qquad \text{(B-23)}$$

To find expansions of $\frac{\cos \psi}{\sin \psi_o}$ and $\frac{\sin \psi}{\sin \psi_o}$ in terms of the first-order and second-order roots, again take $\psi = \psi - \psi_o + \psi_o$. Then,

$$\psi - \psi_o = \mu (\theta - \theta_o) = \left(\mu_n^{(o)} + \frac{\epsilon'}{\theta_o} \right) (\theta - \theta_o)$$

$$= \mu_n^{(o)} (\theta - \theta_o) + \frac{\epsilon'}{\theta_o} (\theta - \theta_o) \qquad \text{(B-24)}$$

$$\psi_o = (2n+1) \frac{\pi}{2} + \epsilon = k \frac{\pi}{2} + \epsilon \quad , \quad k = 1, 3, \ldots \qquad \text{(B-25)}$$

Using (B-24), (B-25) and the fact that ϵ and ϵ' are small, we find

$$\cos \psi = -\sin k\frac{\pi}{2} \left\{ \sin \mu_n^{(o)} (\theta - \theta_o) + \epsilon \frac{\theta}{\theta_o} \cos \mu_n^{(o)} (\theta - \theta_o) \right\} \qquad \text{(B-26)}$$

$$\sin \psi = \sin k\frac{\pi}{2} \left\{ \cos \mu_n^{(o)} (\theta - \theta_o) - \epsilon \frac{\theta}{\theta_o} \sin \mu_n^{(o)} (\theta - \theta_o) \right\} \qquad \text{(B-27)}$$

$$\sin \psi_o = \sin \left((2n+1) \frac{\pi}{2} + \epsilon \right) \approx (-1)^n \qquad \text{(B-28)}$$

Using the results of (B-26), (B-27), and B-28, we find

$$\frac{\mu_n}{\mu_n^2 - \frac{1}{4}} \; B'_{2n}(\theta, \theta_o) i^{-\mu_n} \frac{d}{dx}\left[\left(\frac{x}{ka}\right)^{\frac{1}{2}} J_{\mu_n}(x)\right] (2\pi ka)^{\frac{1}{2}} e^{-i(ka+\frac{\pi}{4})}\Bigg| \tag{B-29}$$

$$\approx \left(\frac{\sin\theta_o}{\sin\theta}\right)^{\frac{1}{2}} \frac{1}{\mu_n^{(o)}\theta_o} \left[\sin \mu_n^{(o)}(\theta - \theta_o) + \frac{1}{\mu_n^{(o)}} \eta_3 \cos \mu_n^{(o)}(\theta - \theta_o)\right] i^{-2\mu_n}$$

$$\eta_3 = \frac{(3 + 4m^2)\cot\theta}{8} \qquad n \gg 1$$

We also take

$$i^{-2\mu_n} = e^{-i(\mu_n^{(o)} + \frac{\epsilon'}{\theta_o})\pi}$$

$$\approx e^{-i\mu_n^{(o)}\pi}\left[1 - i\frac{\epsilon'}{\theta}\pi\right]$$

$$\approx e^{-i\mu_n^{(o)}\pi}\left[1 - \frac{i}{\mu_n(o)}\eta_4\right] \tag{B-30}$$

where

$$\eta_4 = \frac{\pi}{8\theta_o}(3 + 4m^2)\cot\theta_o.$$

Substituting (B-30) in (B-29) and retaining only the two lowest-order terms in $\frac{1}{\mu_n(0)}$, we have for the right-hand side of (B-27)

$$e^{-i\mu_n^{(o)}\pi}\left(\frac{\sin\theta_o}{\sin\theta}\right)^{\frac{1}{2}}\frac{1}{\theta_o}\left\{\frac{\sin\mu_n^{(o)}(\theta-\theta_o)}{\mu_n^{(o)}}+\right. \tag{B-31}$$

$$\left.\frac{1}{(\mu_n^{(o)})^2}\left[\eta_3\cos\mu_n^{(o)}(\theta-\theta_o) - i\,\eta_4\sin\mu_n^{(o)}(\theta-\theta_o)\right]\right\} \qquad n\gg 1$$

After replacing the coefficient $1/\mu_n^{(o)}$ by $\theta_o/n\pi$, the first term in the braces is sumed to give a closed form approximation, $R_{2\phi}(\theta, \theta_o)$, while the last two terms are neglected. Thus,

$$R_{2\phi}(\theta,\theta_o)=\sum_{n=1}^{\infty}R_{2n\phi}(\theta,\theta_o)=\sum_{n=1}^{\infty}\left(\frac{\sin\theta_o}{\sin\theta}\right)^{\frac{1}{2}}\frac{\sin\mu_n^{(o)}(\theta-\theta_o)e^{-i\mu_n^{(o)}\pi}}{n\pi}$$

$$=\frac{-1}{2\pi i}\left(\frac{\sin\theta_o}{\sin\theta}\right)^{\frac{1}{2}}\sum_{n=1}^{\infty}\frac{1}{n}\left[e^{-i\mu_n^{(o)}(\pi-\theta_o+\theta)}-e^{-i\mu_n^{(o)}(\pi+\theta_o-\theta)}\right]$$

$$=\frac{i}{2\pi}\left(\frac{\sin\theta_o}{\sin\theta}\right)^{\frac{1}{2}}\left[g_1(\alpha,\bar{\xi})-g_1(\beta,\bar{\xi})\right] \tag{B-32}$$

where $g_1(\alpha,\bar{\xi})$, $g_1(\beta,\bar{\xi})$ are obtained from $g_1(\alpha,\xi)$, $g_2(\beta,\xi)$ by replacing ξ with $(\xi+1)$.

DISTRIBUTION

Commander
Naval Air Systems Command
Department of the Navy
Washington, D. C. 20360
Attn: AIR-53321A
AIR-360
AIR-50174 (14 cys. /Final only)
AIR-310B (2/Quart. -5/ Final)

Commander
Naval Ordnance Systems Command
Department of the Navy
Washington, D. C. 20360
Attn: NAVSEA-034

Director
Office of Naval Research
800 North Quincy Street
Arlington, Virginia 22217
Attn: ONR-427

Raytheon Company
Missile Systems Division
Hartlwell Road
Bedford, Massachusetts 01730
Attn: Mr. Walter Jeros,
MS S2-32

Commander
Department of the Air Force
Air Force Avionics Laboratory
Electronic Warfare Division
Wright-Patterson Air Force Base
Ohio 45433
Attn: Mr. Harold Weber

Commanding Officer
Naval Air Development Center
Warminster, Pennsylvania 18974
Attn: Mr. Jerry Guarini, AER-2

Director Naval Research Laboratory
Washington, D. C. 20390
Attn: Code 5360
Code 5350
Code 5200
Code 5330

Commanding Officer
Naval Avionics Facility
Indianapolis, Indiana 46218
Attn: Mr. Paul Brink

Commander
Naval Electronics Laboratory Center
San Diego, California 92152
Attn: Code 2330

General Dynamics
Electronics Division
P. O. Box 81127
San Diego, California 92138
Attn: Dr. G. Tricoles

Director
Electro-Sciences Laboratory
Ohio State University
1320 Kinnear Road
Columbus, Ohio 43212
Attn: Mr. Robert Fouty

Sperry-Rand Corporation
Sperry Gyroscope Division
Microwave Engineering Department
Great Neck, New York 11020
Attn: Dr. Robert J. Tims

Commander
Air Force Cambridge Research Lab.
Laurence G. Hanscom Field
Bedford, Massachusetts 01730
Attn: Mr. Philip Blacksmith

McDonnell Douglas Astronautics Co.
5301 Bolsa Avenue
Huntington Beach, California 92647
Attn: Mr. John Wright/Mail Stop 9
Department A3-830/BB10

Teledyne Ryan Company
5650 Kearny Mesa Road
San Diego, California 92119
Attn: Mr. H. Penner

DISTRIBUTION - Continued

Advanced Sensor Laboratory
U.S. Army Missile Command
Redstone Arsenal
Huntsville, Alabama 35809
Attn: Mr. W. Lindberg

Harry Diamond Laboratories
Microwave Research and
Development Branch
Connecticut Avenue and Van Ness Street, N. W.
Washington, D. C. 20438
Attn: Mr. Howard S. Jones, Jr.

Dr. Norbert N. Bojarski
16 Circle Drive
Moorestown, New Jersey 08057

Dr. Alex Hessel
Polytechnic Institute of New York
Route 110
Farmingdale, L.I., N. Y

Dr. Boaz Gelernter
U.S. Army Electronics Command
AMSEL-CT-R
Fort Monmouth, N.J. 07703

Missile Intelligence Agency
U.S. Army Missile Command
Redstone Arsenal
Attn: Mr. R. Thompson (AMSMI/YPE)
Huntsville, Alabama 35809

Stanford Research Institute
Electromagnetic Techniques Laboratory
333 Ravenswood Avenue
Menlo Park, California 94025
Attn: Dr. Don Parker

Dr. R.C. Hansen
Suite 218
17100 Ventura Blvd.
Encino, CA 91316

Unclassified

SECURITY CLASSIFICATION OF THIS PAGE (When Data Entered)

REPORT DOCUMENTATION PAGE		READ INSTRUCTIONS BEFORE COMPLETING FORM
1. REPORT NUMBER	2. GOVT ACCESSION NO.	3. RECIPIENT'S CATALOG NUMBER
4. TITLE (and Subtitle) Pattern Synthesis of Conformal Arrays		5. TYPE OF REPORT & PERIOD COVERED Final Report January 1974 to January 1975
		6. PERFORMING ORG. REPORT NUMBER 2265.30/470, HAC Ref. No. D-0741
7. AUTHOR(s) Peter C. Bargeliotes Alfred T. Villeneuve Wolfgang H. Kummer		8. CONTRACT OR GRANT NUMBER(s) N00019-74-C-0127
9. PERFORMING ORGANIZATION NAME AND ADDRESS Hughes Aircraft Company Culver City, California 90230		10. PROGRAM ELEMENT, PROJECT, TASK AREA & WORK UNIT NUMBERS
11. CONTROLLING OFFICE NAME AND ADDRESS Air Systems Command Department of the Navy Washington, D. C.		12. REPORT DATE January 1975 13. NUMBER OF PAGES 89
14. MONITORING AGENCY NAME & ADDRESS (if different from Controlling Office)		15. SECURITY CLASS. (of this report) Unclassified 15a. DECLASSIFICATION/DOWNGRADING SCHEDULE

16. DISTRIBUTION STATEMENT (of this Report)
Distribution limited to U.S. Agencies only; (Test and Evaluation)(January 1975) Other requests for this document must be referred to Commander, Naval Air Systems Command, AIR-~~310B~~ 954, Washington, D. C 20360

17. DISTRIBUTION STATEMENT (of the abstract entered in Block 20, if different from Report)

18. SUPPLEMENTARY NOTES

19. KEY WORDS (Continue on reverse side if necessary and identify by block number)
Antenna, conformal, conical, array, element, pattern, synthesis, slot, modal series, optical, transition, diffraction, scattering, contour, asymptotic, computer programs.

20. ABSTRACT (Continue on reverse side if necessary and identify by block number)
Exact element patterns computed from expressions of two potential functions representing the modal fields of arbitrary apertures on a conducting cone were compared with measured patterns. Circumferential and radial slots 6.22λ from the tip of a 10° half angle cone were used in the pattern measurements. Measured and computed patterns are in very good agreement. During this same period, an asymptotic approximation of the contour integrals representing the fields of the circumferential

Continued

DD FORM 1 JAN 73 1473 EDITION OF 1 NOV 65 IS OBSOLETE

Unclassified

SECURITY CLASSIFICATION OF THIS PAGE (When Data Entered)

20.

slot was carried out, resulting in approximate expressions for both field components. These expressions describe the component fields in terms of optical, transition and diffraction fields. The diffracted field is a product of a frequency-independent angular function and a simple function containing the position of the radiating element. Such representation of the fields is better suited for numerical computation than the modal series. Recommendations for further investigative work on the topic of conformal arrays are also included.